Chapter 12

# Bioactive Polyaryletherketone Composites

**Ryan K. Roeder, Ph.D.**

*Bioengineering Graduate Program, Department of Aerospace and Mechanical Engineering, University of Notre Dame, Notre Dame, IN, United States*

## 12.1 Introduction

As discussed in detail in previous chapters of this handbook, the clinical and commercial success of polyaryletherketone (PAEK) implants in interbody spinal fusion was enabled by several advantageous properties. PAEK polymers are generally biocompatible, bioinert, and radiolucent; PAEK polymers also exhibit a high strength and similar compliance to bone [1–3]. However, a potential disadvantage is that PAEK alone is neither osteogenic nor bioactive. In interbody spinal fusion, for example, autograft or recombinant human bone morphogenetic protein (e.g., rhBMP-2) is required for osteointegration and, ultimately, for the formation of a bony fusion [2]. Moreover, PEEK implants are often encapsulated with fibrous tissue rather than in direct contact with bone tissue [4–7]. Another potential disadvantage of PAEK polymers is a limited ability to tailor mechanical properties for a particular implant design or to match peri-implant tissue. Bioactive reinforcement particles can be used to simultaneously address both disadvantages by providing (1) bioactivity and (2) tailored mechanical properties.

The addition of bioactive calcium phosphates (CPs)—such as hydroxyapatite (HA), beta-tricalcium phosphate (β-TCP), and bioglass—to polymers offers a robust platform (Fig. 12.1) to engineer implant biomaterials with tailored biological, mechanical, and surgical function [8, 9]. The historical design rationale has been to reinforce a tough, biocompatible polymer matrix with a stiff, bioactive filler. This concept was first investigated by Bonfield and coworkers in the 1980s with the development of HA-reinforced high-density polyethylene (HDPE), which found clinical use under the trade name HAPEX in non-load-bearing otologic and maxillofacial implants [10–13]. The superior mechanical properties of PAEK relative to polyethylene, combined with the clinical and commercial success of PAEK spinal implants in the 1990s, have led to growing interest in bioactive PAEK composites over the last two decades (1999–present, Table 12.1), which will be reviewed in this chapter, highlighted by successful clinical translation of interbody spinal fusion cages composed of HA-reinforced PAEK (Fig. 12.2).

Therefore, the objective of this chapter is to introduce a paradigm for the design of bioactive PAEK composites for biomedical devices (Fig. 12.1) while reviewing the work to date within the framework of that paradigm (Table 12.1). The design of bioactive PAEK composites is considered within the framework of processing-structure-property relationships common to materials science and engineering [61]. The processing, structure, and properties of the material(s) used in a biomedical device have great influence on the device performance. Of course, the device design is also of great importance, but the materials are often chosen "off the shelf" from known commodities without designing the materials for optimal device performance. The policies and practices of the US Food and Drug Administration (FDA) pose limitations to the introduction of new materials but, in this case, PAEK and HA were already well known to the FDA, leading to a relatively straightforward regulatory approval process (510(k) clearance) for implants utilizing bioactive PAEK. Thus, the "simple" combination of PAEK and bioactive CPs offers wide-ranging opportunities to design and manufacture bioactive composites with tailored properties (Fig. 12.1).

**PEEK Biomaterials Handbook.** https://doi.org/10.1016/B978-0-12-812524-3.00012-0

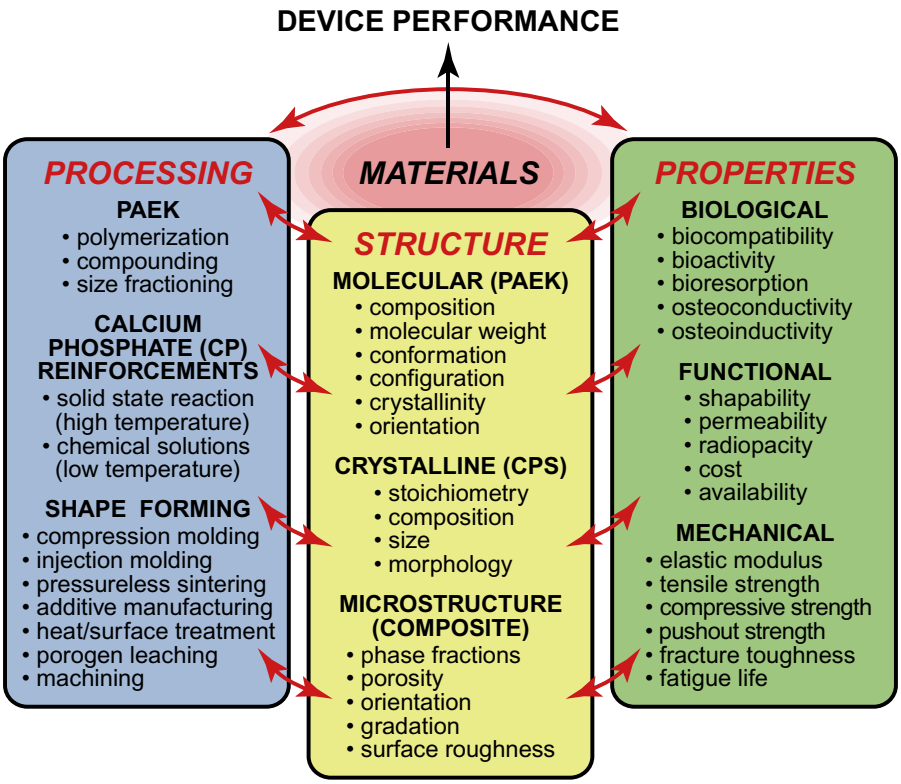


**Figure 12.1** Schematic diagram showing processing-structure-property relationships key to the design of bioactive, calcium phosphate (CP) reinforced PAEK composites for biomedical devices.

## 12.2 Processing-Structure Relationships

### 12.2.1 PAEK Synthesis and Structure

The processing of PAEK beads and powders of varying composition, molecular weight, size, and crystallinity have been reviewed in detail in preceding chapters of this handbook and elsewhere [3, 62]. Investigations of bioactive PAEK composites to date (Table 12.1) have primarily utilized commercial polyetheretherketone (PEEK) beads and powders manufactured by Victrex—grades 150PF [25–27], 150XF [19–23, 28, 29, 63–65], 380G [36, 37], 450G [14–18, 24, 54–57, 62, 66], and 450PF [31, 47, 51–53, 67–70]—and their subsidiary Invibio Biomaterial Solutions under the trade name PEEK-OPTIMA—grades LT1 [7, 49, 50], LT1PF [34, 35], LT3, and LT3UF [34, 71, 72]. The 150 and LT3 grades have a number average molecular weight ($M_n$) of 83,000, while the 450 and LT1 grades have a number average molecular weight of 115,000. Powder grades PF, XF, and UF have a mass average particle diameter ($d_{50}$) of ~50, ~25, and ~10 μm, respectively. A polyetherketoneketone (PEKK) powder with a mean particle size of ~70 μm, manufactured by Oxford Performance Materials (OXPEKK-C), has also been prominently investigated [30–33]. Additional PAEK products have more recently become available from Evonik Industries (Vestakeep PEEK), Solvay Advanced Polymers (Ketaspire and Zeniva PEEK), and Polymics (Arylmax PEEK and PEKK) and are just beginning to be used in research with several published reports since 2015 [73–76]. PAEK polymers were also custom synthesized in several studies [38–41, 77].

### 12.2.2 Bioactive Reinforcement Synthesis and Structure

Bioactive reinforcements or fillers in PAEK composites have primarily utilized crystalline calcium orthophosphates, including stoichiometric HA, non-stoichiometric (calcium-deficient or substituted) HA, and β-TCP (Table 12.2). However, amorphous calcium-containing silicate glasses, including calcium silicate and Bioglass 45S5, have also been utilized for greater solubility. A number of other CPs with varying solubility are also available for use as bioactive reinforcements [86]. A key aspect of

**Table 12.1** Summary of Sustained[a] Published Investigations of Bioactive PEEK Composites Highlighting Processing-Structure-Property Relationships

| Years | Location | References | Processing | ⟷ | Structure | ⟷ | Properties |
|---|---|---|---|---|---|---|---|
| 1999–2009 | Nanyang, Singapore[b] | [14–23] | Melt compounding + injection molding, selective laser sintering, cold press + pressureless sintering | *T* | PEEK + spray dried HA (μm) crystallinity | $V_{HA}$ | Mechanical properties bioactivity cellular response |
| 2006–08 | Erlangen, Germany[c] | [24–27] | Melt compounding + injection molding, selective laser sintering | — | PEEK + β-TCP (μm) PEEK + bioglass 45S5 (μm) porosity | $V_{TCP}$ | Mechanical properties cellular response *in vivo* osteointegration |
| 2007–13 | Notre Dame, USA[d] | [28–35] | Powder mixing + compression molding, + porogen leaching | *T* | PEEK or PEKK + HA whiskers (μm) crystallinity, morphology, preferred orientation, porosity | $V_{HA}$ porosity | Mechanical properties micromechanical modeling permeability |
| 2010–17 | Shenzhen/ Shanghai, PRC[e] | [36–47] | Compounding + injection molding, *in situ* polymerization + sintering or compression molding, powder mixing + compression molding | — | PEEK + nanoscale HA PEEK + $CaO{\cdot}SiO_2$ (μm) crystallinity | $V_{HA}$ | Mechanical properties bioactivity cellular response *in vivo* osteointegration |
| 2012–16 | Hong Kong[f] | [48–50] | Cold press + pressureless sintering, melt compounding + injection molding | — | PEEK + HA nanorods + CNTs crystallinity | $V_{HA}$, $V_{CNT}$ | Mechanical properties bioactivity cellular response |
| 2013–16 | Huainan, PRC[g] | [51–53] | *In situ* precipitation + compression molding | — | PEEK + nanoscale HA FGM | $V_{HA}$, layers | Mechanical properties |
| 2014–15 | Peking, PRC[h] | [54–57] | Compression molding, powder mixing + injection molding, +sand blasting or plasma treatment | — | PEEK + FHA PEEK + HA + carbon fiber surface roughness | Surface roughness | Mechanical properties bioactivity cellular response *In vivo* osteointegration |
| 2016–18 | Changsha, PRC[i] | [58–60] | Selective laser sintering | — | PEEK + HA + GNSs and/or CNTs | $V_{GNS}$, $V_{CNT}$ | Mechanical properties bioactivity *In vivo* osteointegration |

*Abbreviations: β-TCP, beta-tricalcium phosphate; $CaO{\cdot}SiO_2$, calcium silicate; CNT, carbon nanotube; FHA, fluorohydroxyapatite; GNS, graphene nanosheet; HA, hydroxyapatite; PEEK, polyetheretherketone; PEKK, polyetherketoneketone; T, molding temperature; V, phase fractions (vol% or wt%).*

[a] *This summary includes efforts involving at least three publications in reputable scientific journals.*

[b] *Nanyang Technological University, Singapore.*

[c] *Friedrich-Alexander-University, Erlangen-Nuremberg, Erlangen, Germany.*

[d] *University of Notre Dame, Notre Dame, IN, USA.*

[e] *Harbin Institute of Technology and Shenzhen University, Shenzhen, PRC, and Shanghai Jiao Tong University and East China University of Science and Technology, Shanghai, PRC.*

[f] *City University of Hong Kong, Kowloon, Hong Kong.*

[g] *An Hui University of Science and Technology, Huainan, PRC.*

[h] *Peking University, Beijing, PRC.*

[i] *Central South University, Changsha, PRC.*

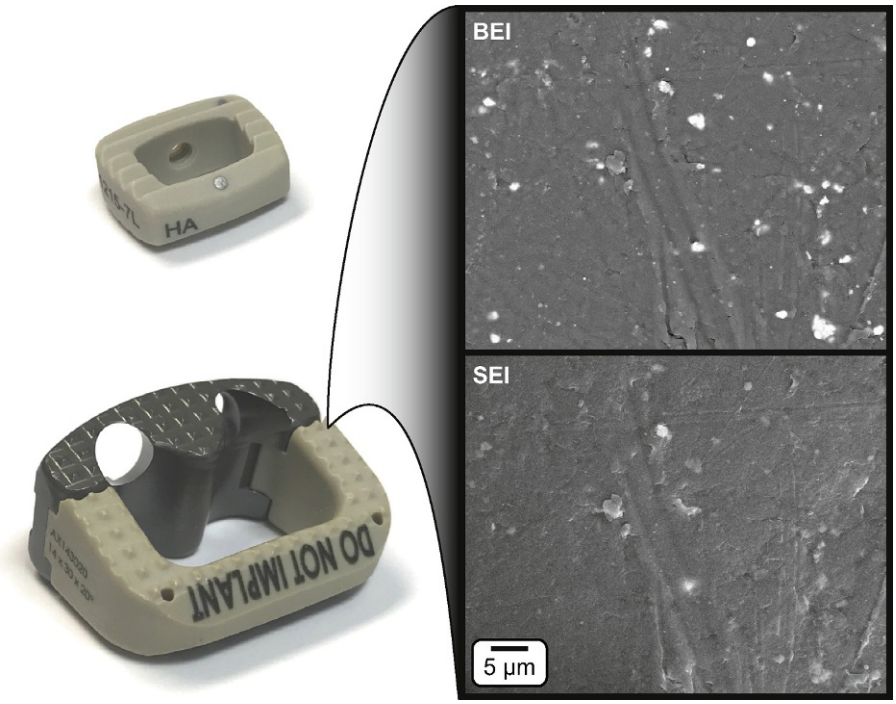


**Figure 12.2** Examples of FDA-approved interbody spinal fusion cages comprising HA-reinforced PAEK (PEEK-Optima HA Enhanced, Invibio, Ltd.), including implants used for anterior cervical interbody fusion (top, Arena-C HA, Spine Frontier, Malden, MA) and stand-alone anterior lumbar interbody fusion (bottom, Ax, Innovasis, Salt Lake City, UT). SEM micrographs using backscattered electron imaging (BEI) and secondary electron imaging (SEI) of the implant surface show HA particles on or near the surface.

selection is the solubility of a particular composition or stoichiometry, which influences biological properties and will be discussed further in Section 12.3.1.

High-temperature synthesis—including solid-state reactions, molten salt synthesis, and spray drying with calcination—generally leads to stoichiometric phases with few crystalline defects and a relatively large crystal size (microscale), though the particle size may be tailored by grinding and/or sorting. Microscale stoichiometric HA, β-TCP, and bioglass particles listed in Table 12.2 were prepared using these methods. Powders prepared by high-temperature solid-state reactions or calcination are generally equiaxed or spherical (Fig. 12.3).

Low-temperature (≤200°C) chemical solution synthesis—including hydrothermal synthesis and precipitation—generally enables greater control over crystal defects (disorder), doping, size, and morphology. Calcium-deficient or substituted HA and calcium silicate particles listed in Table 12.2 were prepared using these methods. Calcium-deficient and substituted HA crystals prepared by low-temperature chemical solution synthesis exhibit greater solubility than stoichiometric HA prepared by high-temperature synthesis (Table 12.2), which may lead to greater bioactivity [87]. Single crystal HA whiskers or platelets, which mimic the morphology of natural apatite crystals in mineralized tissues (Fig. 12.3), have been prepared by hydrothermal synthesis [88–90] and molten salt synthesis [91]. The size of hydrothermally synthesized HA can be tailored from the nanoscale (≤100 nm) [92] to several mm [93].

Lastly, titanium powder was also investigated as a reinforcement or bulk filler in PAEK composites (Table 12.2). The motivation was to improve the bioactivity and osteointegration of PAEK similar to titanium surface coatings discussed in the preceding chapters. However, titanium reinforcements provide inferior biological properties and no advantage in the mechanical properties of PAEK composites compared with calcium orthophosphates and calcium-containing silicate glasses.

## 12.2.3 Composite Manufacturing and Microstructure

A number of processes and pathways have been demonstrated for manufacturing bioactive PAEK composites (Fig. 12.4; Table 12.1). Manufacturing processes can be generalized to include three steps: mixing the bioactive phase with the PAEK polymer, molding composite shapes, and modification of the molded shape. Each process in each step has its own advantages and disadvantages which are discussed below.

### 12.2.3.1 Mixing Processes

Mixing processes have included melt compounding [7, 14–18, 24, 49, 50, 73, 74] and powder mixing (Fig. 12.4). Melt compounding is typically carried

**Table 12.2** Bioactive Reinforcements Used in PAEK Composites, Including Crystalline Calcium Orthophosphates, Amorphous Calcium-Containing Silicate Glasses, and Metals

| Chemical or Trade Name | Chemical Formula[a] | Ca/P | -log($K_{sp}$)[b] | $V$ (vol%)[c] | Morphology | Size | References |
|---|---|---|---|---|---|---|---|
| Calcium hydroxyapatite (HA or HAp) | $Ca_5(PO_4)_3OH$ | 1.67 | 58.3 [78] | ~10<br>0–40 | Equiaxed<br>spherical | $d_{50}$ = 4–6 μm<br>$d_{50}$ ~ 20–100 μm | [7, 71, 72]<br>[14–23, 66, 67] |
| Calcium-deficient HA | $Ca_{5-x/2}(HPO_4)_{x/2}(PO_4)_{3-x/2}(OH)_{1-x/2}$ | 1.5–1.67 | ~42.6 [79] | 0–50<br>0–40 | Whiskers<br>nanoparticles | ~23 × 3 μm<br>~20–100 nm | [28–35]<br>[36–53, 55–59, 65, 73–75, 80][d] |
| Calcium fluorohydroxyapatite (FHA) | $Ca_5(PO_4)_3F_x(OH)_{1-x}$ | 1.67 | 59.1–62.2 [81][e] | 0, 30 | Nanoparticles | <100 nm | [54] |
| Substituted HA (M-HA, $M^{2+}$ = Sr or Ce) | $M_xCa_{5-x}(PO_4)_3OH$ | 1.5–1.67 | n/r | 0–30 | Equiaxed | $d_{50}$ = 43 μm | [65, 77] |
| Beta-tricalcium phosphate (β-TCP) | β-$Ca_3(PO_4)_2$ | 1.5 | 28.9 [82] | 0–22 | Equiaxed | <63 μm<br><1 μm | [24–27]<br>[60] |
| Calcium silicate | $CaO{\cdot}SiO_2{\cdot}H_2O$ | n/a | 13.8–23.2 [83][f] | 0–50 | Equiaxed | n/r | [42, 46, 64] |
| Bioglass 45S5 | $CaO{\cdot}P_2O_5{\cdot}Na_2O{\cdot}SiO_2$[g] | n/a | n/r | 0–20 | Equiaxed | <50–60 μm<br>~100–500 nm | [26, 63]<br>[68, 69, 84, 85] |
| Titanium | Ti | n/a | Insoluble | 0–60 | Irregular | $d_{50}$ ~ 27 μm | [70] |

*Abbreviations: $d_{50}$ = mean or median particle diameter, $K_{sp}$ = solubility product, n/a = not applicable, n/r = not reported.*
[a] *0 < x < 1.*
[b] *Solubility product measured or calculated at 25°C.*
[c] *Values reported in wt% were converted to vol% using known or assumed densities for PAEK and the bioactive phase.*
[d] *These studies did not report a Ca/P ratio but can be assumed to be calcium-deficient HA based upon the synthesis methods.*
[e] *This range reflects x ~ 0–1.*
[f] *This range reflects Ca/Si ~ 1.0–1.6.*
[g] *Bioglass 45S5 is composed of 45 wt% CaO, 6.0 wt% $P_2O_5$, 24.5 wt% $Na_2O$, and 24.5 wt% $SiO_2$.*

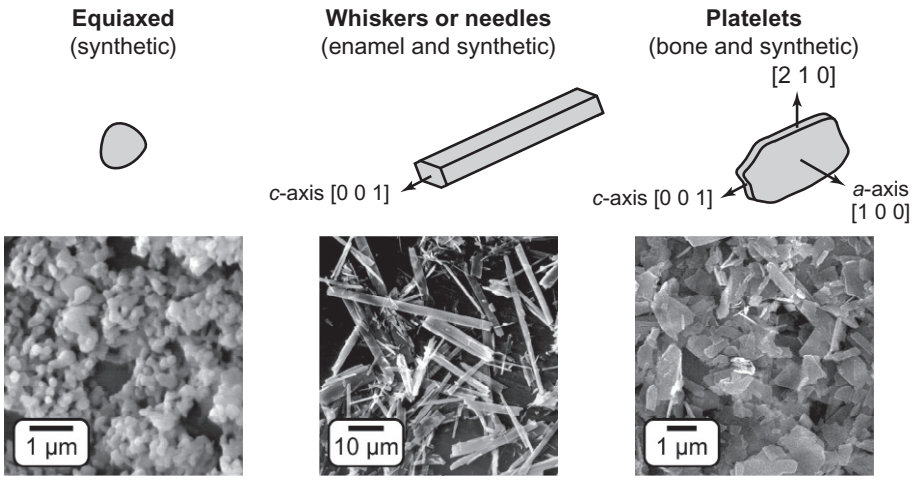


**Figure 12.3** Schematic diagram (not to scale) showing common morphologies of natural and synthetic hydroxyapatite (HA) crystals. The SEM micrographs show equiaxed HA crystals prepared by calcination, as well as whisker and plate-like calcium-deficient HA crystals prepared by hydrothermal synthesis.

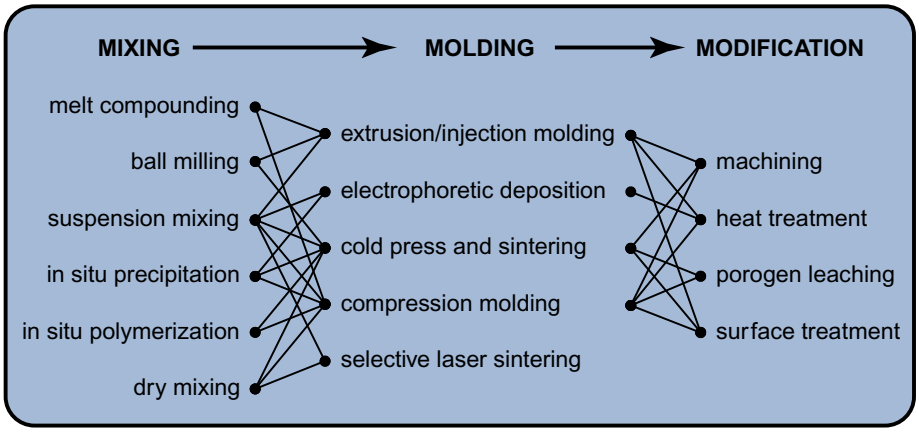


**Figure 12.4** Schematic diagram showing various processes and pathways for manufacturing bioactive PAEK composites. Manufacturing processes can be generalized to include three steps: mixing the bioactive phase with PAEK polymers, molding composite shapes, and modification of the molded shape. Linkages show pathways that have been demonstrated in published reports.

out in a conventional twin-screw extruder and is thus well suited for low cost, high volume commercial manufacturing. Standard PAEK beads may be used, rather than powders, since bioactive reinforcements are mixed into the molten polymer by shear flow during compounding. However, an increased melt viscosity with the addition of inorganic reinforcements limits reliable mixing and molding to less than 30–40 vol%, and high reinforcement fractions may also cause excessive wear on equipment.

Powder mixing processes can be further subdivided into ball milling [23, 36, 37, 41, 42, 46, 64], suspension mixing [28–35, 43, 48, 54–60, 63, 65, 68, 69, 75, 76, 84, 85], *in situ* precipitation [51–53, 77, 80], *in situ* polymerization [38–40, 45], and dry mixing [19–22, 25–27, 67, 70] (Fig. 12.4). Ball milling is straightforward and scalable, but the powder mixture must be separated from the milling media and may become contaminated by the milling media. Suspension mixing has been most widely utilized due to facilitating uniform dispersion of multiple micro- and/or nanoscale powders within a fluid, such as ethanol or water. Mixing commonly includes stirring and/or ultrasonic dispersion to break apart particle agglomerates. Ethanol can be advantageous over water for preventing dissolution of bioactive reinforcements or salt porogen particles, for rapid solvent evaporation upon drying the mixed powder, and for sterilization. *In situ* precipitation and polymerization are processes similar to suspension mixing except that one phase (e.g., the bioactive particles) is mixed in the suspension and the other phase (e.g., the PAEK polymer) is either precipitated or polymerized within the suspension to form an intimate mixture. Dry mixing powders using a tumbler or shaker is advantageous in avoiding the use of a fluid and the extra step of collecting the powder mixture from the fluid. However, suspension mixing of powders, specifically by *in situ* precipitation, was shown to result in improved dispersion compared with dry mixing, as evidenced by significantly improved mechanical strength of the resultant PAEK composites [52].

### 12.2.3.2 Molding Processes

Molding processes have included extrusion [7], injection molding [15–18, 24, 36, 37, 41, 42, 46, 49, 50, 55–57, 66, 68, 69, 74], electrophoretic deposition [63, 77], cold pressing and pressureless sintering [22, 23, 40, 48, 64, 84, 85], compression molding [27–35, 43, 45, 47, 51–54, 65, 70–73, 75, 76], and selective laser sintering (SLS) [19–21, 25–27, 58–60] (Fig. 12.4). Extrusion and injection molding are amenable to low cost, high volume commercial manufacturing of net shapes with a dense microstructure. Melt compounding is typically used to mix bioactive reinforcements with standard PAEK beads prior to extrusion or injection molding. Importantly, the recent commercialization of PEEK Optima HA-Enhanced (Invibio, Ltd.) was facilitated by melt compounding and extrusion of bar stock which is supplied to manufacturers for machining implants (Fig. 12.2), as discussed further below.

Electrophoretic deposition has been used in a couple studies to apply a bioactive PAEK composite coating to nitinol [63] or stainless steel [77]. Electrophoretic deposition allows powder mixing and molding to be combined into a single step, but is limited to coatings deposited on a conductive electrode and requires subsequent heat treatment to densify the deposited particles.

Cold pressing and pressureless sintering has low overhead equipment costs and is amenable to almost any level of reinforcement during processing. However, an extended sintering time may require a controlled (inert gas) atmosphere to prevent oxidation of PAEK. HA-reinforced PEEK composites were able to be sintered at a temperature (325°C) well below the melting temperature of PEEK, but required 15 h for densification [23]. The absence of applied pressure during sintering results in residual microporosity on the size scale of the starting powders. This residual microporosity may be beneficial for fluid entrapment and cell attachment, but is detrimental to mechanical properties [23, 48].

Compression molding is similar to injection molding in relatively low cost, high volume commercial manufacturing of net shapes with a dense microstructure, except that production rates are lower and machining may be required to attain non-geometric shapes. Like cold pressing and pressureless sintering, compression molding is amenable to nearly any level of reinforcement during processing and is highly adaptable to a wide array of upstream mixing processes and downstream modifications (Fig. 12.4). However, unlike cold pressing and pressureless sintering, the resultant microstructure is fully dense, resulting in improved mechanical properties. For these reasons, compression molding has been investigated as a flexible manufacturing platform for bioactive PAEK composites and implants of varying size, shape, and macroporosity [31] (Fig. 12.5).

The SLS offers low overhead equipment costs and customizable net shape manufacturing from image files (computed tomography or computer-aided design) with geometric freedom that is not possible with injection molding or machining. SLS is thus especially suited for manufacturing macroporous scaffolds with tailored architecture. Interestingly, manufacturing of bioactive PAEK composites and microporous scaffolds by SLS was first demonstrated [19–21] long before the recent growth of interest in additive manufacturing, or three-dimensional (3D) printing, of medical plastics and implants. The main limitations of SLS are a high cost due to a relatively slow production rate and, even more critically, an inability to reuse most of the extra PAEK in the powder bed, such that more than 50% of the costly PAEK powder feedstock is relegated to waste. Also, the maximum reported porosity and reinforcement volume fraction have been limited to 70–74 vol% and 22 vol%, respectively [21], which was noted to be at least partly due to poor mechanical integrity [19, 20]. Moreover, the porosity is dependent on the reinforcement content and laser power [21]. Finally, carbon black powder (~1 wt%) is typically added to PAEK powders to aid in laser heating and powder flow during SLS.

The molding temperature and time are critical for each of the preceding molding methods. Moreover, the molding temperature is the primary, and arguably only, processing parameter that has been systematically investigated [14, 19, 23, 28, 32–34] for processing-structure relationships (Fig. 12.1). Excessive temperature and time can cause oxidation of PAEK polymers, while inadequate temperature and time can lead to poor densification and mechanical integrity. Thermal history also has a significant influence on the crystallinity of PAEK polymers [3, 62]. Increased melt temperature resulted in significantly decreased crystallinity in dense HA-reinforced PEEK (Victrex 450G) [14]. In compression-molded HA-reinforced PEEK scaffolds, increased mold temperature resulted in decreased crystallinity for a

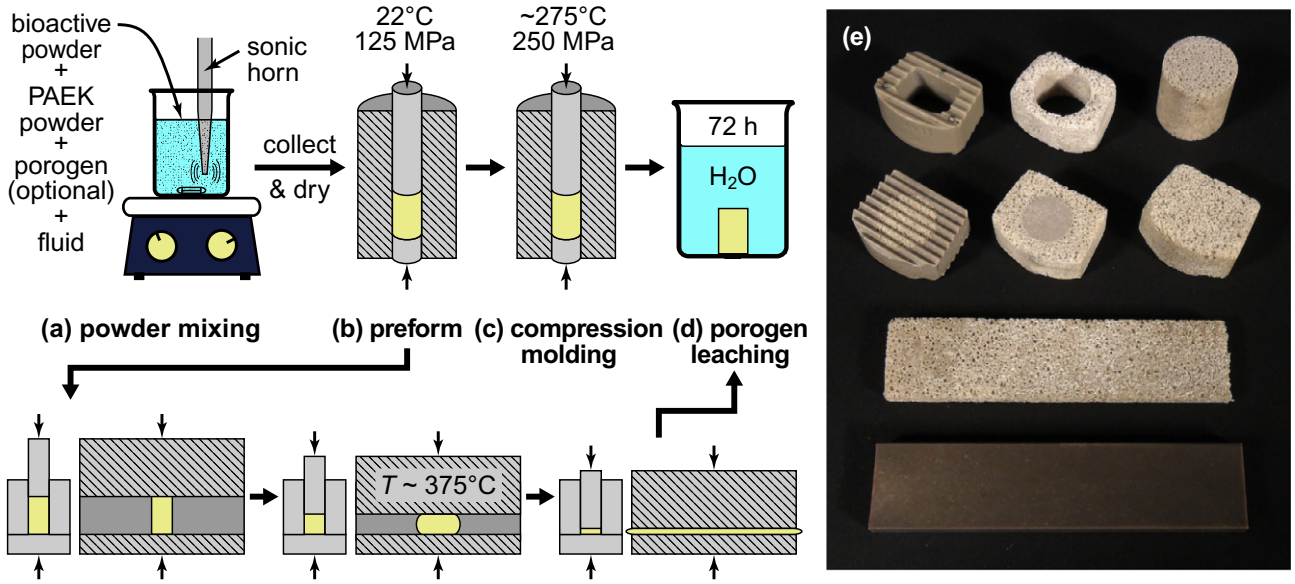


**Figure 12.5** Schematic diagram showing compression molding as a flexible manufacturing platform for bioactive and porous PAEK composites and implants. The process steps include: (a) wet powder mixing in suspension, (b) cold pressing a composite preform, (c) compression molding in dies designed for controlled flow and final shapes, and (d) leaching the porogen (if applicable). (e) Photograph showing various examples of dense and/or macroporous bioactive PAEK composites and implants of varying size and shape produced by (a–d), compared to a commercial cervical interbody spinal fusion cage (upper left). All specimens comprised PEEK (Invibio LT1) reinforced with 20 vol% calcium-deficient HA whiskers and were molded either fully dense or with 75 vol% porosity using a sodium chloride porogen. Note that the dense beam at the bottom has dimensions of $43 \times 10 \times 2.5$ mm.

higher molecular weight PEEK with a larger particle size (Invibio LT1PF or Victrex 450PF), but a maxima in crystallinity at 360–365°C for a lower molecular weight PEEK with a smaller particle size (Invibio LT3UF or Victrex 150UF) [34]. The overall results of this study suggested that HA-reinforced PEEK scaffolds should be compression molded at 370–375°C [34].

### 12.2.3.3 Modification

Modification subsequent to molding has included machining [7, 31], heat treatment [16, 28–30, 37, 63, 68, 69, 74], porogen leaching [17, 31–35, 71, 72, 75, 76, 84, 85], and various surface treatments [24, 55–57, 75, 76] (Fig. 12.4). Bioactive PAEK composites are readily machined using standard tooling after extrusion, injection molding, cold pressing and sintering, or compression molding processes. Commercial manufacturing of bioactive PAEK interbody spinal fusion cages (Fig. 12.2) relies on computer numerical control (CNC) machining of various implant designs and footprints from extruded bar stock of PAEK compounded with HA particles (PEEK Optima HA-Enhanced, Invibio, Ltd.). This approach ensures (1) the supply of consistent material while allowing implant manufacturers freedom to customize implant designs and footprints, and (2) bioactivity of all implant surfaces as HA particles are exposed upon machining the bulk material (Fig. 12.2). The effects of machining and tooling parameters on HA exposure are thus critical to implant performance, but have not been reported. Preclinical research has also demonstrated that porous and bioactive PAEK scaffolds are readily machined prior to leaching the porogen [31], as shown by grooves milled onto the top surface of an implant shown in Fig. 12.5.

Heat treatment may be necessary or advantageous following any of the preceding molding processes in order to relieve residual stresses and/or tailor the PAEK crystallinity. An annealing treatment above the glass transition temperature of PEEK (143°C) has been shown to be beneficial for some mechanical properties and the homogeneity of HA-reinforced PEEK [16, 28, 74]. This effect was most likely due to relieving residual stress and controlling recrystallization, evidenced by a measured increase in crystallinity [74]. In as-molded composites, the measured crystallinity of PEEK ranged from 22% to 31% and exhibited little or no change with increased levels of HA reinforcement [14, 37, 67, 74]. However, more detailed investigation revealed that PEEK

crystallinity in the outermost "skin" of injection-molded composites was unaffected (20–22%), but crystallinity in the bulk "core" region of composites increased from 24% to 31% with 0–40 vol% HA reinforcement [15]. In a separate study, the thickness of the "skin" was shown to be increased with an increased injection flow rate [74]. Differences in the core/skin are not unexpected due to differences in cooling rate, and were subsequently minimized by an annealing treatment [74]. Overall, there has been relatively little investigation on the effects of the cooling rate or annealing treatment on the crystallinity of bioactive PAEK composites, as well as the presence or effects of an interphase layer adjacent to reinforcement particles. This is surprising considering their known importance in carbon fiber-reinforced PEEK [94].

Porogen leaching has been used to create tailored macroporosity in molded bioactive PAEK composites and implants to enhance osteointegration via bone ingrowth. Injection molding, cold pressing and sintering, and compression molding have been augmented with porogen leaching to produce macroporous PAEK scaffolds (Figs. 12.4 and 12.5). A sacrificial porogen phase (e.g., sodium chloride particles) is simply mixed or compounded with the PAEK and bioactive reinforcements prior to molding and then removed by dissolving in a solvent after molding [31–35, 84, 85]. HA microspheres have also been utilized as a porogen phase in PAEK polymers [71, 72, 75, 76]. The porogen phase must exhibit thermal stability at or near the melting temperature of PAEK polymers and solubility in a solvent in which PAEK is insoluble.

Surface treatments have included controlling surface roughness via polishing [24, 54] or sand blasting [55–57], surface microporosity via sulfonation of PAEK [75, 76], and surface bioactivity via plasma treatment [56] or HA deposition [75, 76]. The primary motivation for each of these treatments is to provide additional improvement in the biological properties (e.g., bioactivity) of PAEK composites beyond that provided by the bioactive reinforcements alone. As such, these surface treatments had been primarily investigated for PAEK well before being borrowed for bioactive PAEK composites, and are thus discussed in greater detail in preceding chapters of this handbook and elsewhere. Polishing and sand blasting treatments have been utilized to investigate the effects of surface roughness on biological properties, which are discussed below, but little attention has been given to effects on surface exposure of the bioactive phase. PAEK polymers can be sulfonated to create surface microporosity [95] that may be advantageous for fluid entrapment, cell attachment, and osteointegration. Plasma treatments have been shown to significantly improve the wettability of PAEK polymers via surface oxidation, but effects on the bioactivity and osteointegration of PAEK polymers have been modest or not significant [56, 96, 97]. Finally, HA has been deposited within the microporosity of sulfonated PAEK via immersion in simulated body fluid (SBF) [75, 76], which differs from conventional thermal spray approaches for applying solid HA coatings to PAEK polymers.

#### 12.2.3.4 Microstructural Characterization

Quantitative microstructural characterization has mainly included the density of the composite; the crystallinity of PAEK; the volume fraction, size, morphology, and preferred orientation of bioactive reinforcements; and the porosity of scaffolds. The bulk density, apparent density, and porosity of PAEK composites can be measured accurately on small samples [21, 28, 29, 32, 48, 71, 84, 85] using standardized methods based upon Archimedes principle [98, 99]. The PAEK crystallinity has been measured in bioactive PAEK composites using differential scanning calorimetry (DSC) [14, 15, 37, 48, 50, 67, 70, 74] or Fourier transform infrared (FTIR) spectroscopy [34]. DSC provides a bulk measurement where standardized methods [100] remove the effect of prior thermal history [62], while FTIR can be used to probe the as-molded microstructure [101].

The volume fraction, size, morphology, and preferred orientation of bioactive reinforcements can be measured in microscopy using standard stereological methods [102]. Alternatively, if the PAEK polymer can be pyrolyzed at a temperature where the bioactive reinforcements are unaffected, reinforcements in the composite can removed from the PAEK matrix after molding such that the volume fraction, size, and morphology of reinforcements can be measured using gravimetric analysis and microscopy both before and after molding [15, 29, 103]. Degradation in the length and aspect ratio of HA whisker reinforcements after extrusion and compression molding were statistically characterized using these methods [29, 103]. The crystallographic and morphological orientation of the same single crystal HA whisker

reinforcements in PEEK was characterized using quantitative texture analysis by X-ray diffraction (XRD) [9, 28, 29]. Interestingly, viscous flow during compression molding produced a mechanically advantageous preferred orientation of HA whiskers along the length of test specimens which was similar to that exhibited by apatite crystals in human cortical bone tissue along the direction of principal stress [28].

Dispersion of reinforcements in the PAEK matrix and test specimen fracture surfaces have been typically assessed qualitatively from optical or electron micrographs. By this assessment, microscale bioactive reinforcements have been readily dispersed within PAEK polymers using various mixing and molding processes (Fig. 12.4, Table 12.1). However, dispersion of nanoscale reinforcements, especially at more than 10 vol%, has been more challenging due to high surface area and attractive surface forces resulting in microscale agglomerates that persist in as-molded composites [44] and thus negate the potential advantage of nanoscale reinforcements. Therefore, various powder suspension mixing methods have been used to improve the dispersion of nanoscale bioactive reinforcements in PAEK polymers with varying degrees of success [44].

The exposure of bioactive reinforcements on as-molded and machined PAEK surfaces has been qualitatively observed from SEM micrographs [7, 9, 22–27, 32–34, 36–46, 54–60, 63, 64, 70, 74, 80, 84, 85] and von Kossa staining [32]. In SEM, backscattered electron imaging is advantageous due to atomic number contrast between CP reinforcements and the PAEK matrix, but can be misleading because backscattered electrons penetrate the specimen surface to a depth of ~1 μm such that image contrast is apparent for CP particles located just beneath a thin layer of PAEK at the surface. Thus, some CP particles may appear to be exposed when they are not, and this can be appreciated by directly comparing backscattered electron images with secondary electron images (Fig. 12.2). Secondary electrons penetrate the specimen surface <100 nm and are excellent for imaging of surface topography but provide little atomic number contrast. Thus, given the critical importance of the surface exposure of bioactive reinforcements for bioactivity and osteointegration of PAEK composites, standardized methods are needed for quantitative characterization of surface exposure. Unfortunately, the broad fluorescence emission spectrum of PEEK, ranging from 400 to 600 nm [55], interferes with common fluorophores (e.g., alizarin, calcein) that could be used to label calcium.

The volume, architecture, and interconnectivity of porosity in bioactive PAEK scaffolds is critical for *in vivo* osteointegration, as discussed below, and has been quantitatively characterized using micro-computed tomography (micro-CT) [32, 35, 71, 75] and mercury porosimetry [75, 84]. Guidance into these and other methods for characterizing scaffold porosity is available elsewhere [104]. In HA whisker-reinforced PAEK scaffolds with 75–90% porosity (Fig. 12.5), segmented micro-CT images were used to verify that >99% of porosity was interconnected and to measure the mean pore size (~200–300 μm), strut thickness (~40–90 μm), anisotropy, and strut morphology [32, 35]. Increased porosity resulted in decreased strut thickness and more rod-like struts [32, 35], while increased HA content resulted in increased strut thickness [32].

In summary, there is a continued need for quantitative microstructural characterization in order to establish structure-property relationships and rationally design bioactive PAEK composites. A "make it and break it" approach (processing-property relationships) that does not pay careful attention to the composite microstructure [61] will be detrimental to continued progress.

## 12.3 Structure-Property Relationships

### 12.3.1 Biological Properties

PAEK polymers are well known to be biocompatible and bioinert [2–4, 96, 105–109]. PAEK and carbon fiber-reinforced PAEK were encapsulated by a layer of fibrous tissue *in vivo* after intramuscular implantation in rabbits [4, 106], subcutaneous implantation in sheep [108], fixation of a canine femoral osteotomy [106], and injection of particles into the spinal canal of rabbits [107]. PAEK and carbon fiber-reinforced PAEK were partially encapsulated by fibrous tissue in distal femoral and proximal tibial defects in sheep [96], as well as interbody spinal fusion of sheep [2] and goats [110], although the interbody spinal fusion implants were augmented with osteoinductive autograft or rhBMP-2. Retrievals of failed spinal fusion cages in humans exhibited an absence of direct bone apposition to carbon fiber-reinforced PAEK implants [5].

CPs, on the other hand, are well known to be biocompatible and bioactive [87, 111–116]. Bioactivity is the ability of a biomaterial to elicit or modulate a favorable response ("activity") from any part of a biological organism [61]. For example, HA is well known to enhance osteoblastic differentiation *in vitro* [117]. CPs consistently exhibit direct apposition of bone tissue, without the use of autograft or BMPs, no matter whether implanted in osseous defects [87, 112] or non-osseous sites [112–116]. In the latter case of subcutaneous or intramuscular implantation, CPs may be considered osteoinductive. The bioactivity and osteoinductivity of CPs *in vivo* has been attributed to chemotactic signaling to cells due to the release of calcium ions by dissolution and/or osteoclastic resorption, as well as an affinity for binding osteoinductive proteins from the implant site [112, 113].

Therefore, the solubility product ($K_{sp}$) is a key consideration in the choice of a bioactive phases (Table 12.2). Solubility may not only aid bioactivity through calcium release and cellular signaling, but may also lead to complete degradation of bioactive reinforcements. Degradation of reinforcements may be desirable in the case of degradable polymer composites. However, PAEK polymers are not degradable and thus PAEK composites are intended to function as permanent implants. Therefore, the complete degradation of bioactive reinforcements in PAEK composites could lead to a loss of biological and/or mechanical function. After 86 weeks in a mini-pig trabecular bone defect, 97% of a β-TCP bone substitute was completely removed [118]. This suggests that for long-term function bioactive reinforcements in PAEK composites should comprise stoichiometric HA, calcium-deficient HA, or substituted HA, which exhibit slow resorption over a period of years [87, 111]. The solubility and bioactivity of HA is generally increased with increased defects in the crystal structure, including ionic substitutions, and decreased particle size [87, 112, 119].

#### 12.3.1.1 *In Vitro* Investigations

Early investigations of bioactive PAEK composites primarily focused on *in vitro* assessments of bioactivity and cytocompatibility (Table 12.1). After immersion in SBF, a layer of carbonated apatite was deposited on PAEK reinforced with stoichiometric HA [21, 22], calcium-deficient HA [57, 65], fluorohydroxyapatite (FHA) [54], Sr-HA [65], calcium silicate [42, 64], or bioglass [68, 69, 84, 85], but not PAEK alone, confirming that these reinforcements provide bioactivity and the PAEK matrix is bioinert. The thickness and surface coverage of the deposited apatite layer increased with increased HA [22, 48, 65] or calcium silicate [64] content. Strontium-substitution (Sr-HA) further enhanced the *in vitro* bioactivity of HA [65], while substitution with strontium and cerium (Sr,Ce-HA) further enhanced *in vitro* bioactivity beyond either dopant alone [77]. *In vitro* bioactivity was also further enhanced with increased porosity (and thus surface area) in bioactive PAEK scaffolds [84, 85]. Note that in order to avoid interference from the bioactive reinforcements in the underlying composite, the apatite layer should be removed from the composite surface for characterization using XRD, FTIR, and other surface analytical techniques [22].

The water contact angle was decreased for PAEK reinforced with HA [50], FHA [41, 54], and calcium silicate [42] compared with PAEK alone, indicating that bioactive reinforcements improved surface wettability or hydrophilicity. Moreover, the contact angle decreased, or surface wettability increased, with increased calcium silicate content in PAEK [42]. The contact angle was further decreased with increased surface roughness superimposed on HA-reinforced PEEK surfaces [55], and with the addition of surface microporosity via sulfonation [75, 76] or HA deposition via SBF immersion [76].

Cell attachment, viability (or metabolic activity), proliferation, differentiation [or alkaline phosphatase (ALP) activity], and mineralization on bioactive PAEK composites has been investigated using human fibroblasts [21], murine fibroblasts [57], human osteoblasts (hOBs) [24], human fetal OBs (hFOBs) [25, 26], immortalized human OB precursor cells (MG-63 [54–57, 65, 77, 80], SaOS-2 [48]), immortalized murine OB precursor cells (MC3T3-E1) [41, 42, 48–50, 69, 70, 84, 85], human bone marrow-derived stromal cells (hBMSCs) [71, 72], human adipose-derived stromal cells (hASCs) [74], and rabbit BMSCs [75]. Cells are typically cultured for up to 14 days, and sometimes even 28 days for investigating differentiation and mineralization. Bioactive PAEK composites have consistently exhibited cytocompatibility in supporting cell attachment, metabolic function, proliferation, differentiation, and mineralization, without exception for all bioactive reinforcements listed in Table 12.2.

Osteoblast (hFOB, MC3T3-E1, MG-63), fibroblast, and hASC attachment, viability, proliferation,

ALP activity, and/or mineralization was generally improved for HA [41, 48–50, 54, 57, 65, 74], calcium silicate [42], and bioglass [26, 84, 85] reinforced PEEK, but not β-TCP-reinforced PEEK [24–26], compared with PEEK alone. Moreover, osteoblast (SaOS-2, MC3T3-E1) viability, ALP activity, and/or mineralization were progressively increased with increased HA [48, 49] or bioglass [84] content in PEEK. Osteoblast (MG-63) mineralization was stronger for Sr-HA compared with HA reinforcements [65]; osteoblast (MC3T3-E1) viability, as well as antimicrobial activity, was enhanced on strontium and cerium substituted HA (Sr,Ce-HA) compared with either dopant alone [77]. Antibacterial properties were reported for Sr and/or Ce substituted HA [77], as well as FHA [54]. Osteoblast (MC3T3-E1) viability and ALP activity was also improved for titanium-reinforced PEEK compared with PEEK alone [70], but the effect was small compared with CPs.

The effects of additional modifications to bioactive PAEK composites have also been investigated. The addition of 1 wt% carbon black to aid particle flow in SLS [25, 26], as well as up to 20 wt% carbon reinforcements (fibers, nanotubes, and graphene) to enhance mechanical properties [49, 50, 55–59, 68, 69], did not diminish the cytocompatibility or bioactivity of CP-reinforced PAEK composites. In fact, osteoblast (MC3T3-E1) viability and ALP activity was reported to be progressively increased with increased carbon nanotube (CNT) content at fixed bioglass content in PEEK [69]. Osteoblast (MG-63) attachment, viability, ALP activity, and mineralization was further improved with increased surface roughness superimposed on HA-reinforced PEEK surfaces [54–56]. The addition of macroporosity [75] or microporosity [85] via porogen leaching, surface microporosity via sulfonation [75], and HA deposition via SBF immersion [75] were reported to further improve the cell (MC3T3-E1, BMSC) viability and/or ALP activity of bioactive PAEK composites.

As with all *in vitro* investigations of cell behavior, the interpretation of results and comparison between the preceding studies must carefully consider differences in cell type, cell seeding density, culture media, time points, and substrate surface roughness, among other factors, especially when confronted with what appear to be confounding and/or spurious results. Biological assays commonly utilize fluorophores (e.g., alizarin, calcein, fluorescein isothiocyanate, rhodamine) for labeling proteins and mineralization. Therefore, careful consideration must also be given to possible interference from the broad fluorescence emission spectrum of PEEK, spanning 400–600 nm [120], when selecting assays and designing experiments with necessary control groups. Systematic investigations designed for direct comparison of the effects of the bioactive reinforcement composition, size, morphology, and surface exposure will be important for continued progress.

#### 12.3.1.2 *In Vivo* Investigations

*In vivo* osteoconductivity or osteointegration of bioactive PAEK composites has been investigated in a number of preclinical models, including ovine cervical interbody fusion [7], ovine femoral and tibial defects [7], porcine cranial defects [27], rat femoral defects [40, 45, 76], rabbit cranial defects [46], rabbit femoral defects [47, 84, 85], canine dental implants [54–57], and rabbit radial defects [59, 60]. The study duration is dependent on the model but is typically 8–16 weeks, although two studies were carried out between 24 and 26 weeks [7, 27]. Overall, bioactive PAEK composites have consistently exhibited osteoconductivity, osteointegration, and direct apposition of both cortical and cancellous bone (Fig. 12.6).

The first significant study reporting *in vivo* osteointegration of bioactive PAEK composites utilized PEEK reinforced with 4 vol% β-TCP prepared by SLS that was implanted into 10 mm diameter porcine cranial defects [27]. The thickness of the fibrous tissue layer encapsulating the implant decreased with increased β-TCP content and time post-implantation. At 24 weeks post-implantation, there was direct apposition of bone to β-TCP reinforcements but not the PEEK matrix. Moreover, the push-out strength of β-TCP-reinforced PEEK implants was 13 times greater than that for PEEK alone [22]. An earlier study reported bone ingrowth into a porous HA-reinforced PEEK scaffold prepared by SLS at 16 weeks post-implantation in pigs [19], but no further details were provided.

A number of studies have also reported that bioactive PAEK composites exhibited improved osteointegration and bone contact compared with PAEK alone, which is surrounded by fibrous tissue. These reports include HA-reinforced PEEK in rat femoral defects at 3 months [40], HA- and FHA-reinforced PEEK dental implants in the canine mandible at 4–12 weeks [54, 57], HA- and calcium silicate-reinforced PEEK in ovine cranial defects at 8 weeks

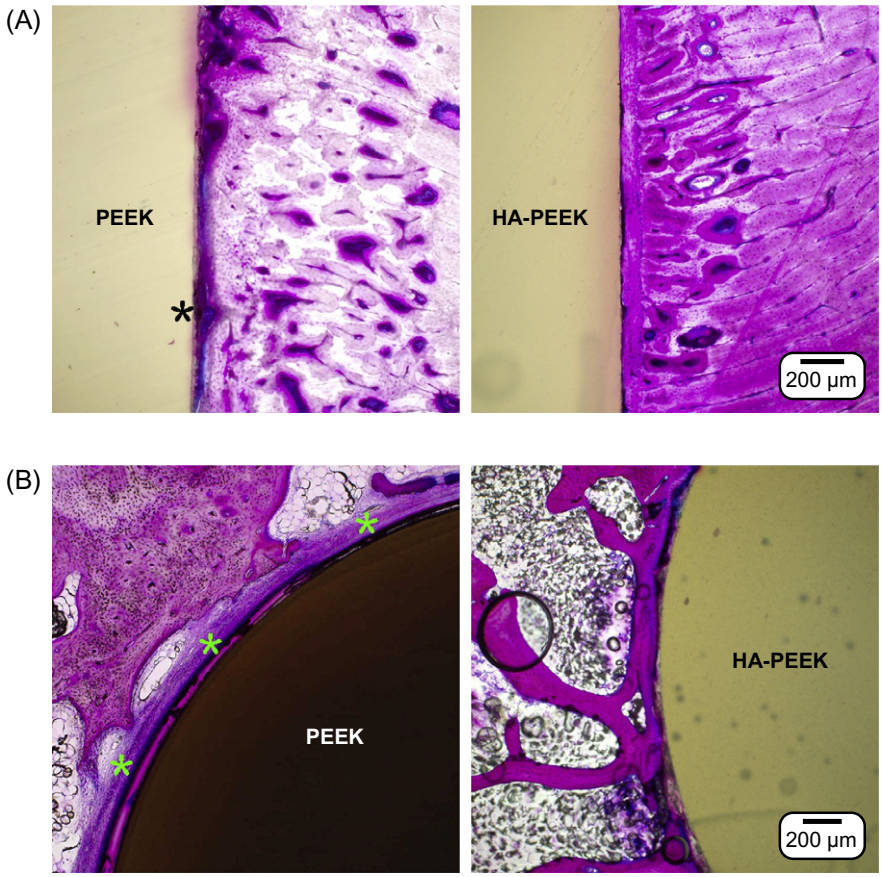


**Figure 12.6** Optical micrographs of histological sections showing (A) cortical and (B) cancellous bone ongrowth to PEEK and HA-reinforced PEEK (PEEK Optima HA-Enhanced, Invibio Ltd.) after 12 weeks of implantation in ovine femoral and tibial defects. PEEK exhibited a fibrous tissue interface (*) whereas HA-reinforced PEEK exhibited direct bone contact. Adapted from W.R. Walsh, M.H. Pelletier, N. Bertollo, C. Christou, C. Tan, Does PEEK/HA enhance bone formation compared with PEEK in a sheep cervical fusion model? Clin. Orthop. Relat. Res. 474 (2016) 2364–2372 with permission.

[46], HA-reinforced PEEK in rabbit tibial defects at 16 weeks [47], macroporous bioglass-reinforced PEEK in rabbit distal femoral defects at 12 weeks [84, 85], and HA-reinforced PEEK (PEEK Optima HA-Enhanced, Invibio Ltd.) in ovine femoral and tibial defects at 4–12 weeks (Fig. 12.6) [7]. Importantly, PEEK Optima HA-Enhanced (Invibio, Ltd.) also exhibited improved osteointegration and bone contact compared with PEEK alone in ovine cervical interbody fusion at 6–12 weeks [7]. New bone formation and bone contact was greater for PEEK reinforced with calcium silicate compared with HA after 8 weeks implantation in ovine cranial defects [46]. This result was explained by the greater solubility of calcium silicate; *in vitro* release of calcium was greater for calcium silicate compared with HA [46]. Recall, however, that the benefit of greater solubility in the near term must be weighed against a complete loss of the bioactive phase in the long term, which has not been investigated. The push-out strength and new bone formation measured for PEEK reinforced with ~2 vol% HA was surprisingly not improved with increased HA content (up to 15 vol%) after 16 weeks of implantation in rabbit tibial defects, likely due to agglomeration of HA particles in the PEEK matrix or the chosen time point [47]. In contrast, new bone formation was increased with increased bioglass content in macroporous PEEK after 12 weeks of implantation in rabbit distal femoral defects [84].

The effects of additional modifications to bioactive PAEK composites have also been investigated. The addition of 1 wt% carbon black to aid particle flow in SLS [22], as well as up to 20 wt% carbon reinforcements (fibers, nanotubes, and graphene) to enhance mechanical properties [55–57], has not been appeared to have detrimental effect on *in vivo* osteointegration of CP-reinforced PAEK composites, but direct comparison of bioactive PAEK composites with and without carbon additives is lacking. Osteointegration and bone contact was further improved with increased surface roughness superimposed on HA-reinforced PEEK surfaces implanted in the canine mandible at 4 weeks [55, 56]. The addition of macroporosity via porogen leaching, surface microporosity

via sulfonation, and HA deposition via SBF immersion were reported to further improve the osteointegration and push-out strength of PAEK after 2–12 weeks of implantation in rat distal femoral defects [76]. Interestingly, these effects were also significantly greater in PEKK compared with PEEK, which was suggested to be due to the greater number of ketone groups being more sensitive to sulfonation and HA deposition treatments [76]. The addition of microporosity was also reported to further improve new bone formation in macroporous bioglass-reinforced PEEK after 3 months of implantation in rabbit distal femoral defects [85].

Osteointegration is preferably characterized by quantitative measures in histology or micro-CT, such as the new bone volume to total volume ratio (BV/TV), bone mineral density (BMD), trabecular thickness (TbTh), and trabecular number (TbN), among others [46, 54–57, 76, 84]. Bone apposition or contact is preferably characterized by quantitative measures in histology, such as the surface area or percent of the surface in direct contact [46, 76]. The best metric for osteointegration may be the mechanical integrity of the bone-implant interface, which can be measured using a push-out test, but surprisingly few studies have used this [19, 47, 76]. Systematic investigations designed for direct comparison of the effects of the bioactive reinforcement composition, size, morphology, and surface exposure will be important for continued progress.

### 12.3.2 Functional Properties

Other functional properties of importance for bioactive PAEK composites include intraoperative shapability, hydraulic permeability, radiopacity, cost, and availability. Dense PAEK composites could conceivably be shaped intraoperatively using a high-speed burr, while porous PAEK composites could also be shaped intraoperatively using a scalpel or rongeur. The hydraulic permeability of bioactive PEEK scaffold was measured using forced fluid flow and Darcy's law [35]. Permeability was increased with increased porosity, as expected. Importantly, permeability was greater for scaffolds prepared with an ellipsoidal versus cubic pore morphology that was imparted from the porogen morphology [35]. CP reinforcement does not detract from the advantageous radiolucency of PAEK in postoperative radiographic assessment, but may be used instead of barium sulfate to enable radiographic visualization of an implant. For example, PAEK reinforced with 40–50 vol% HA exhibits X-ray attenuation similar to human cortical bone. Finally, just as the greater cost of PAEK polymers over conventional biomedical thermoplastics was proved to be justified by enhanced performance, the added cost of raw materials and manufacturing bioactive PAEK composites must be justified by additional performance benefits. Commercialization of PEEK Optima HA-Enhanced (Invibio, Ltd.) was facilitated by adapting existing manufacturing methods for PEEK, which minimized additional costs to that of supplying the HA filler. The availability of PAEK polymers from a variety of suppliers in a variety grades and forms, as listed in Section 12.2.1, is advantageous for the development of new medical devices. CPs and other bioactive fillers are presently not as readily available as PAEK polymers, but commercial suppliers nonetheless exist.

### 12.3.3 Mechanical Properties

The mechanical properties of bioactive PAEK composites have been evaluated by static uniaxial tension [15–18, 23, 24, 28, 36–39, 41–43, 47–50, 52, 54, 55, 57, 66, 68–70, 73, 74], cyclic uniaxial tension [17, 18, 74], static uniaxial compression [23, 31, 33–35, 41, 42, 52, 58–60, 70–73, 84], implant push-out strength [27, 47, 76], ultrasonic wave propagation [28, 29], static four-point bending [65], cyclic four-point bending [30], static three-point bending [48, 53, 64, 68, 69, 73], Izod impact testing [74], and micromechanical models [29, 121–123]. Bioactive PAEK composites have exhibited excellent static mechanical properties and fatigue properties compared to other polymers (Fig. 12.7). Both dense and macroporous PAEK composites using all types of bioactive reinforcements (Table 12.2), but primarily HA, have been engineered to mimic mechanical properties exhibited by human cortical and trabecular bone tissue, respectively (Table 12.3).

Dense HA-reinforced PAEK composites have been engineered to mimic the longitudinal elastic modulus of human cortical bone at a similar volume fraction of HA [15–18, 28] (Table 12.3), whereas other polymers with bioactive reinforcements were only able to mimic the transverse elastic modulus of human cortical bone (Fig. 12.7a). Numerous studies have reported an increased elastic modulus with increased reinforcement content, as expected and shown by the overall trend for HA-PAEK composites

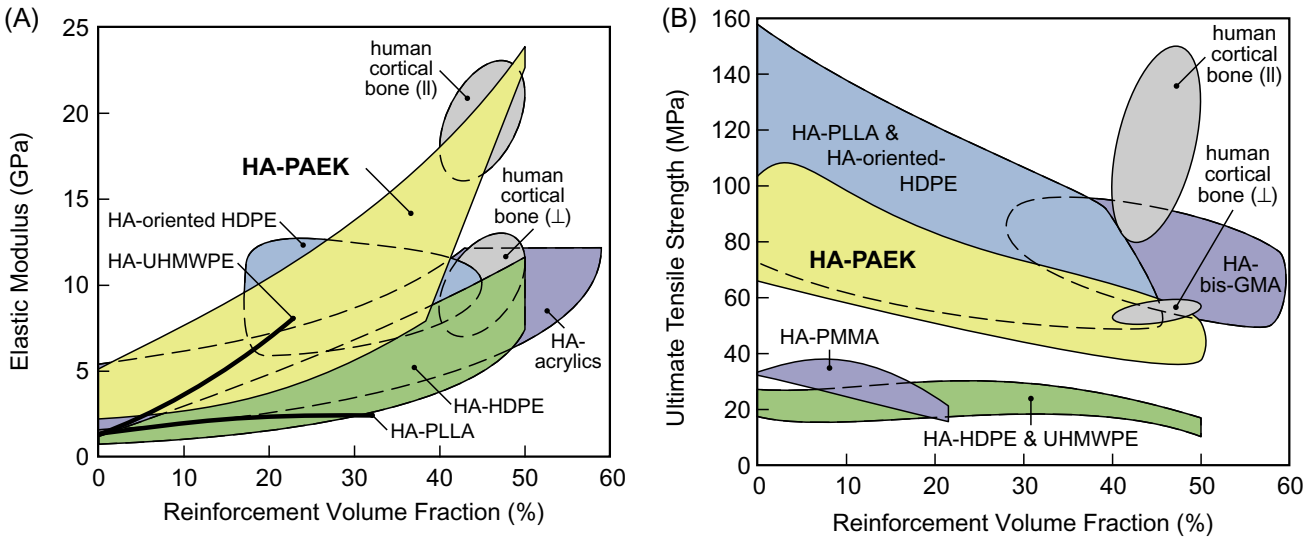


**Figure 12.7** (A) Elastic modulus and (B) ultimate tensile strength of human cortical bone tissue compared with HA-reinforced PAEK and other polymers relevant to orthopedic implants. Note that the regions are shown to simplify and be inclusive of a large number of data points from the literature for high-density polyethylene (HDPE) [10, 12, 124], PAEK [15–18, 28, 39, 41, 42, 48, 52, 54, 74], ultrahigh molecular weight polyethylene (UHMWPE) [125], acrylics—including polymethyl methacrylate (PMMA) [126–128] and bisphenol-*a*-glycidyl methacrylate/triethylene glycol dimethacrylate (bis-GMA/TEG-DMA) [129–132]—PLLA [133, 134], and anisotropic (oriented) HDPE [135–138]. The mechanical properties of cortical bone are shown for loading parallel (II) and perpendicular (⊥) to the longitudinal anatomic axis [138, 139]. The data set was limited to uniaxial tensile tests to allow comparison without confounding effects of the testing methods (e.g., bending tests).

**Table 12.3** Dense HA Reinforced PAEK Composites Have Exhibited an Elastic Modulus (*E*) and Ultimate Tensile Strength (*UTS*) Similar to Human Cortical Bone Tissue, While Macroporous HA or Bioglass Reinforced PAEK Composite Scaffolds Have Exhibited an Apparent Compressive Elastic Modulus (*E*) and Yield Strength (*YS*) Similar to That of Human Vertebral Trabecular Bone

| **Uniaxial Tension** | **Porosity (%)** | **Apatite Content (vol%)** | ***E* (GPa)** | ***UTS* (MPa)** |
|---|---|---|---|---|
| Dense HA-PAEK [15–18, 28, 39, 41, 42, 48, 52, 54, 74] | ~0 | 0–50 | 2–23 | 40–110 |
| Human cortical bone (longitudinal) [138, 139] | ~5–10 | ~40 | 16–23 | 80–150 |
| **Uniaxial Compression** | **Porosity (%)** | **Apatite Content (vol%)** | ***E* (MPa)** | ***YS* (MPa)** |
| Macroporous HA- or bioglass-PAEK [33–35, 75, 84] | 70–90 | 0–40 | 1–880 | 0.01–32 |
| Human vertebral trabecular bone [140, 141] | ~80–95 | ~40 | 20–500 | 0.5–4 |

in Fig. 12.7a. Dense HA-reinforced PAEK composites have also achieved the transverse ultimate tensile strength of human cortical bone at a similar volume fraction of HA [15–18, 28, 41, 42], similar to other polymers, and have reached the low end of the longitudinal ultimate tensile strength of human cortical bone at lower levels of reinforcement (Fig. 12.7b). Numerous studies have reported decreased ultimate tensile strength with increased reinforcement content, as shown by the overall trend for HA-PAEK composites in Fig. 12.7b. Bioactive reinforcements act as flaws in the polymer matrix due to limited

interfacial bonding. Therefore, a design trade-off exists between increased bioactivity and stiffness, but decreased strength and ductility, with increased levels of bioactive reinforcements. The inherent trade-off can be mitigated by improving load transfer from the matrix to reinforcement. Therefore, researchers have investigated the bioactive reinforcement morphology, nanoscale reinforcements, chemical coupling, and the addition of carbon-based reinforcements.

Elongated reinforcements (e.g., fibers) are well known to improve the load transfer from the matrix to the reinforcement. The use of single crystal, elongated HA whiskers was previously shown to result in significantly improved tensile and fatigue properties when directly compared to conventional, equiaxed HA powder reinforcements in HDPE composites [124, 142]. Compression molded HA whisker-reinforced PEEK (Victrex 150XF) [28] exhibited a greater elastic modulus and ultimate tensile strength compared to injection molded HA powder-reinforced PEEK (Victrex 450G) [15–18]. The difference in PEEK molecular weight was opposite the difference in mechanical properties; therefore, this difference was most likely due to the HA reinforcement morphology, but may have also been influenced by differences in PEEK crystallinity. The HA whisker-reinforced PEEK composites were orthotropic [28, 29] due to a preferred orientation of the HA whiskers in the direction of flow during molding in a channel die (Fig. 12.5). The degree of preferred orientation and elastic anisotropy were tailored to be similar to human cortical bone [28] and were strongly correlated [29].

The high specific surface of nanoparticles (<100 nm) is potentially advantageous for cell attachment and mechanical reinforcement. Therefore, and not surprisingly, a large number of studies have investigated PAEK reinforced with HA nanoparticles [36–59, 65, 73–75, 80] (Tables 12.1 and 12.2). Unfortunately, the reported mechanical properties of nanoscale HA-reinforced PAEK have not exceeded those reported for microscale HA-reinforced PAEK. The primary pitfall has been agglomeration of nanoscale reinforcements due to difficulty dispersing nanoparticles in PAEK polymers [44]. Indeed, microscale agglomerates of nanoparticles provide little or no benefit over microscale particles as reinforcements. Despite the large number of investigations on nanoscale reinforcements, studies designed for direct comparison of the effects of reinforcement size on the mechanical properties of bioactive PAEK composites are surprisingly lacking.

Silane coupling agents are widely used in composites and have been investigated for improving interfacial bonding between the PAEK matrix and HA reinforcements [43, 47, 66, 73]. Silane coupling improved the elastic modulus, tensile strength, and ductility of HA-reinforced PAEK [43, 47, 58, 66], but unfortunately the reported differences have been relatively modest. Coupling agents will need to result in more dramatic improvements in mechanical properties in order to justify added cost and regulatory scrutiny.

The addition of up to ~20 wt% carbon fibers [55, 57], ~8 wt% CNTs [49, 50, 68, 69], and ~1 wt% graphene nanosheets (GNSs) [58, 59] has been investigated as a means to further enhance the mechanical properties of bioactive PAEK composites. The addition of CNTs and GNSs improved tensile properties compared with the bioactive PAEK composite alone [49, 50, 58, 59, 68, 69], but not beyond what has been achieved with a similar level of additional bioactive reinforcements (Fig. 12.7). The elastic modulus and tensile strength were reported to initially increase with increased CNT or GNS reinforcement, but reached a maxima at 1–4 wt% [50, 58, 59, 69]. This suggests that, similar to nanoscale HA reinforcements, the limitation may be agglomeration of CNTs and GNSs within the PAEK matrix. In contrast, the addition of ~20 wt% short carbon fibers (~100 μm in length) to PEEK reinforced with ~10 vol% (25 wt%) nanoscale HA exhibited a tensile modulus of ~16.5 GPa and ultimate tensile strength of ~136 MPa [55, 57]. This tensile modulus is comparable to PAEK reinforced with 40 vol% microscale HA [15–18, 28] and the reported tensile strength significantly exceeds that of any bioactive PAEK composite alone (Fig. 12.7b). Thus, a mixture of HA and carbon fibers may enable both bioactivity and bone-like stiffness while further improving strength.

Micromechanical models have been used to study the effects of the reinforcement morphology and orientation on anisotropic elastic constants [29], the effects of the HA/PAEK interface on the composite mechanical properties [121, 122], and the progressive damage behavior of microporous HA-reinforced PAEK scaffolds [123]. Once validated against experimental data, micromechanical models can be useful for designing new bioactive PAEK composites for improved performance and elucidating the mechanisms underlying structure-property relationships.

For example, a multilevel micromechanical model that accounted for the orientation distribution of HA whiskers in PAEK composites was able to more accurately predict the orthotropic elastic constants compared to common, idealized assumptions of randomly oriented or perfectly aligned reinforcements [29]. Stress-strain curves for dense [121, 122] and macroporous [123] HA-reinforced PAEK composites were accurately predicted using multilevel finite element models accounting for matrix and interface damage, rather than assuming a perfectly adhesive interface.

In tension-tension fatigue, injection molded HA powder-reinforced PEEK exhibited a fatigue strength at 1 million cycles of approximately 60, 50, 40, 35, and 30 MPa for 0, ~4, 10, 20, and 30 vol% HA, respectively [17, 18, 74]. The applied stress was typically at least 50% of the ultimate tensile strength. Composites failed by debonding of the HA/PEEK interface, followed by initiation and growth of microcracks which accumulated to form a fatigue crack [18]. The residual elastic modulus and ultimate tensile strength following fatigue to 1 million cycles was decreased by 5–30% and 15–25%, respectively, for 0–30 vol% HA [18]. In four-point bending fatigue, compression molded HA whisker-reinforced PEKK exhibited a fatigue strength at 2 million cycles of approximately 75, 60, and 40 MPa for 0, 20, and 40 vol% HA whiskers, respectively [30]. Fig. 12.8 shows a representative fatigue failure surface of PEKK reinforced with 20 vol% HA whiskers.

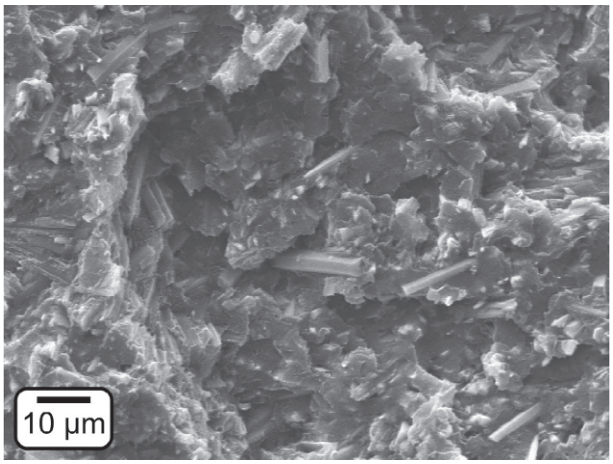


**Figure 12.8** SEM micrograph showing a representative failure surface for PEKK (OXPEKK-C) reinforced with 20 vol% HA whiskers after loading in cyclic four-point bending fatigue. HA whisker are visible embedded or protruding from the PEKK matrix.

Last but not least, macroporous HA-reinforced PAEK composites have been engineered to mimic the compressive modulus and strength of human vertebral trabecular bone [33–35, 75, 84] (Table 12.3). The earliest and most rigorous investigations to date focused on PEKK [31, 33] and PEEK [34, 35] scaffolds prepared by compression molding and porogen leaching (Fig. 12.5) with 75–90 vol% porosity and 0–40 vol% HA whisker reinforcements. Increased porosity resulted in a nonlinear decrease in the compressive modulus and yield strength [33], as expected, and a cubic vs. ellipsoidal pore morphology did not have a significant effect on mechanical properties [35]. The mechanical properties were generally maximum and most reliable at 20 vol% HA reinforcement [33]. The compressive modulus, yield strength, and yield strain increased with increased mold temperature [33, 34] to a maxima at ~375–385°C due to improved densification [34]. PEKK scaffolds with 75% porosity and 20 vol% HA molded at 375°C exhibited a mean compressive modulus and yield strength of 149 and 2.2 MPa, respectively, which was the highest of the conditions investigated and similar to human vertebral trabecular bone (Table 12.3).

More recent investigations of macroporous HA-reinforced PAEK composites have explored lower porosity levels and alternate reinforcement strategies to achieve greater mechanical strength. Bioactive PEKK [75] scaffolds prepared by compression molding and porogen leaching with 70 vol% bulk porosity, and surface treated by sulfonation and HA deposition, exhibited a compressive yield strength of ~21–32 MPa [75]. Similarly, PEEK scaffolds prepared by cold pressing, sintering, and porogen leaching with 2–21 vol% bioglass reinforcements and 70%–85% porosity were reported to exhibit an ultimate compressive strength of ~6–8 MPa [84]. PEEK scaffolds prepared by SLS with ~4–10 vol% HA and ~0–1 wt% CNT or GNS reinforcements were reported to exhibit a compressive modulus of 2–4 GPa and compressive strength of ~35–80 MPa [58, 59], but the level of porosity was not reported and likely relatively low for bone ingrowth. Continued progress in understanding and engineering structure-property relationships in bioactive PAEK scaffolds requires more careful characterization of the scaffold architecture which typically has a greater effect than the reinforcement phase.

## 12.4 Concluding Remarks

This chapter reviewed key results and accomplishments from nearly two decades (1999–present) of work on bioactive PAEK composites, and did so within the framework of processing-structure-property relationships. There has been considerable expansion of research efforts and commercial interest in bioactive PAEK composites from the first decade to the second decade (Table 12.1). Documented research efforts for bioactive PAEK composites began with one paper published in 1999 [14] and continued with at least 20 more papers in the first decade (1999–2008) followed by at least 50 more papers in the second decade (2009–2018). The recent advent of bioactive PAEK interbody spinal fusion cages (Fig. 12.2), supported by a growing body of scientific literature reporting the advantages of bioactive PAEK composites for *in vivo* osteointegration (e.g., Fig. 12.6), combined with growing interest in macroporous bioactive PAEK scaffolds, will fuel continued growth of this field into its third decade.

Bioactive PAEK composites are poised for continued growth in the interbody spinal fusion market and expansion into new clinical applications, including suture anchors, synthetic bone graft substitutes, fracture fixation devices, and dental implants, among others. The limited supply and risks associated with autograft and allograft tissue, combined with the cost and recent scrutiny by the FDA for the use of rhBMP-2 in cervical spinal fusion [143], will continue to provide ample clinical and commercial motivation in the spine market. Now that HA-reinforced PAEK (Fig. 12.2) and porous PAEK [144] have been implemented in FDA-approved interbody spinal cages, bioactive *and* porous PAEK devices are expected to follow, as predicted a decade ago [31].

Despite at least 70 published reports to date on bioactive PAEK composites, as reviewed in this chapter, many key processing-structure-property relationships are still only beginning to be established. Gaps in the current state of knowledge for bioactive PAEK composites were noted throughout this chapter. Foremost among these, the effects of processing methods on bioactive reinforcement surface exposure, and subsequent effects of surface exposure on bioactivity and osteointegration, require attention. Moreover, given its critical importance on biological function, standardized methods are needed for quantitative characterization of surface exposure. There exists a general continued need for quantitative microstructural characterization in order to establish structure-property relationships and rationally design bioactive PAEK composites. Systematic investigations designed for direct comparison of the effects of the bioactive reinforcement composition, size, morphology, and surface exposure on *in vitro* bioactivity and *in vivo* osteointegration will be important for continued progress.

## References

[1] S. L. Evans, P. J. Gregson, Composite technology in load-bearing orthopaedic implants, Biomaterials 19 (1998) 1329–1342.

[2] J. M. Toth, M. Wang, B. T. Estes, J. L. Scifert, H. B. Seim III, A. S. Turner, Polyetheretherketone as a biomaterial for spinal applications, Biomaterials 27 (2006) 324–334.

[3] S. M. Kurtz, J. N. Devine, PEEK biomaterials in trauma, orthopedic, and spinal implants, Biomaterials 28 (2007) 4845–4869.

[4] D. F. Williams, A. McNamara, R. M. Turner, Potential of polyetheretherketone (PEEK) and carbon-fibre-reinforced PEEK in medical applications, J. Mater. Sci. Lett. 6 (1987) 188–190.

[5] D. Togawa, T. W. Bauer, I. H. Lieberman, H. Sakai, Lumbar intervertebral body fusion cages: histological evaluation of clinically failed cages retrieved from humans, J. Bone Joint Surg. 86A (2004) 70–79.

[6] P. J. Rao, M. H. Pelletier, W. R. Walsh, R. J. Mobbs, Spine interbody implants: material selection and modification, functionalization and bioactivation of surfaces to improve osseointegration, Orthop. Surg. 6 (2014) 81–89.

[7] W. R. Walsh, M. H. Pelletier, N. Bertollo, C. Christou, C. Tan, Does PEEK/HA enhance bone formation compared with PEEK in a sheep cervical fusion model? Clin. Orthop. Relat. Res. 474 (2016) 2364–2372.

[8] K. Rezwan, Q. Z. Chen, J. J. Blaker, A. R. Boccaccini, Biodegradable and bioactive porous polymer/inorganic composite scaffolds for bone tissue engineering, Biomaterials 27 (2006) 3413–3431.

[9] R. K. Roeder, G. L. Converse, R. J. Kane, W. Yue, Hydroxyapatite reinforced polymer biocomposites for synthetic bone substitutes, JOM 60 (2008) 38–45.

[10] W. Bonfield, M. D. Grynpas, A. E. Tully, J. Bowman, J. Abram, Hydroxyapatite reinforced polyethylene - a mechanically

compatible implant material for bone replacement, Biomaterials 2 (1981) 185–186.
[11] K. E. Tanner, R. N. Downes, W. Bonfield, Clinical applications of hydroxyapatite reinforced materials, Br. Ceram. Trans. 93 (1994) 104–107.
[12] M. Wang, R. Joseph, W. Bonfield, Hydroxyapatite-polyethylene composites for bone substitution: effects of ceramic particle size and morphology, Biomaterials 19 (1998) 2357–2366.
[13] L. D. Silvio, M. J. Dalby, W. Bonfield, Osteoblast behaviour on HAP/PE composite surfaces with different HA volumes, Biomaterials 23 (2002) 101–107.
[14] M. S. Abu Bakar, P. Cheang, K. A. Khor, Thermal processing of hydroxyapatite reinforced polyetheretherketone composites, J. Mater. Process. Technol. 89-90 (1999) 462–466.
[15] M. S. Abu Bakar, P. Cheang, K. A. Khor, Tensile properties and microstructural analysis of spheroidized hydroxyapatite-poly (etheretherketone) biocomposites, Mater. Sci. Eng. A 345 (2003) 55–63.
[16] M. S. Abu Bakar, P. Cheang, K. A. Khor, Mechanical properties of injection molded hydroxyapatite-polyetheretherketone biocomposites, Compos. Sci. Technol. 63 (2003) 421–425.
[17] M. S. Abu Bakar, M. H. W. Cheng, S. M. Tang, S. C. Yu, K. Liao, C. T. Tan, K. A. Khor, P. Cheang, Tensile properties, tension-tension fatigue and biological response of polyetheretherketone-hydroxyapatite composites for load-bearing orthopedic implants, Biomaterials 24 (2003) 2245–2250.
[18] S. M. Tang, P. Cheang, M. S. A. Bakar, K. A. Khor, K. Liao, Tension-tension fatigue behavior of hydroxyapatite reinforced polyetheretherketone composites, Int. J. Fatigue 26 (2004) 49–57.
[19] K. H. Tan, C. K. Chua, K. F. Leong, C. M. Cheah, P. Cheang, M. S. Abu Bakar, S. W. Cha, Scaffold development using selective laser sintering of polyetheretherketone-hydroxyapatite biocomposite blends, Biomaterials 24 (2003) 3115–3123.
[20] K. H. Tan, C. K. Chua, K. F. Leong, C. M. Cheah, W. S. Gui, W. S. Tan, F. E. Wiria, Selective laser sintering of biocompatible polymers for applications in tissue engineering, Biomed. Mater. Eng. 15 (2005) 113–124.
[21] K. H. Tan, C. K. Chua, K. F. Leong, M. W. Naing, C. M. Cheah, Fabrication and characterization of three-dimensional poly (ether-ether-ketone)/-hydroxyapatite biocomposite scaffolds using laser sintering, J. Eng. Med. 219 (2005) 183–194.
[22] S. Yu, K. P. Hariram, R. Kumar, P. Cheang, K. A. Khor, *In vitro* apatite formation and its growth kinetics on hydroxyapatite/polyetheretherketone biocomposites, Biomaterials 26 (2005) 2343–2352.
[23] C. Hengky, B. Kelsen, P. C. Saraswati, Mechanical and biological characterization of pressureless sintered hydroxyapatite-polyetheretherketone biocomposite, ICBME Proc. 23 (2009) 261–264.
[24] L. Petrovic, D. Pohle, H. Münstedt, T. Rechtenwald, K. A. Shlegel, S. Rupprecht, Effect of βTCP filled polyetheretherketone on osteoblast cell proliferation *in vitro*, J. Biomed. Sci. 13 (2006) 41–46.
[25] D. Pohle, S. Ponader, T. Rechtenwald, M. Schmidt, K. A. Shlegel, H. Münstedt, F. W. Neukan, E. Nkenke, C. von Wilmowsky, Processing of three-dimensional laser sintered polyetheretherketone composites and testing of osteoblast proliferation *in vitro*, Macromol. Symp. 253 (2007) 65–70.
[26] C. von Wilmowsky, E. Vairaktaris, D. Pohle, T. Rechtenwald, R. Lutz, H. Münstedt, G. Koller, M. Schmidt, F. W. Neukam, K. A. Shlegel, E. Nkenke, Effects of bioactive glass and β-TCP containing three-dimensional laser sintered polyetheretherketone composites on osteoblasts *in vitro*, J. Biomed. Mater. Res. 87A (2008) 896–902.
[27] C. von Wilmowsky, R. Lutz, U. Meisel, S. Srour, S. Rupprecht, T. Toyoshima, E. Nkenke, K. A. Shlegel, D. Pohle, H. Münstedt, T. Rechtenwald, M. Schmidt, *In vivo* evaluation of β-TCP containing 3D laser sintered poly(ether ether ketone) composites in pigs, J. Bioact. Compat. Polym. 24 (2009) 169–184.
[28] G. L. Converse, W. Yue, R. K. Roeder, Processing and tensile properties of hydroxyapatite-whisker-reinforced polyetheretherketone, Biomaterials 28 (2007) 927–935.
[29] J. M. Deuerling, J. S. Vitter, G. L. Converse, R. K. Roeder, Micromechanical model for the orthotropic elastic constants of polyetheretherketone composites considering the orientation distribution of the hydroxyapatite

whisker reinforcements, J. Eng. Mater. Technol. 134 (2012) 010906 (8 pages).
[30] G. L. Converse, T. L. Conrad, R. K. Roeder, Fatigue life of hydroxyapatite whisker reinforced polyetherketoneketone, Trans. Soc. Biomater. 32 (2009) 584.
[31] R. K. Roeder, S. M. Smith, T. L. Conrad, N. J. Yanchak, C. H. Merrill, G. L. Converse, Porous and bioactive PEEK implants for interbody spinal fusion, Adv. Mater. Process. 167 (2009) 46–48.
[32] G. L. Converse, T. L. Conrad, C. H. Merrill, R. K. Roeder, Hydroxyapatite whisker-reinforced polyetherketoneketone bone ingrowth scaffolds, Acta Biomater. 6 (2010) 856–863.
[33] G. L. Converse, T. L. Conrad, R. K. Roeder, Mechanical properties of hydroxyapatite whisker reinforced polyetheretherketone composite scaffolds, J. Mech. Behav. Biomed. Mater. 2 (2009) 627–635.
[34] T. L. Conrad, D. J. Jaekel, S. M. Kurtz, R. K. Roeder, Effects of the mold temperature on the mechanical properties and crystallinity of hydroxyapatite whisker-reinforced polyetheretherketone scaffolds, J. Biomed. Mater. Res. 101B (2013) 576–583.
[35] T. L. Conrad, C. H. Merrill, R. K. Roeder, Effects of an ellipsoidal versus cubic pore morphology on the permeability, mechanical properties, and cell infiltration of HA reinforced PEEK scaffolds, in: First International PEEK Meeting, Philadelphia, PA, 2013.
[36] L. Wang, L. Weng, S. Song, Q. Sun, Mechanical properties and microstructure of polyetheretherketone–hydroxyapatite nanocomposite materials, Mater. Lett. 64 (2010) 2201–2204.
[37] L. Wang, L. Weng, S. Song, Z. Zhang, S. Tian, R. Ma, Characterization of polyetheretherketone-hydroxyapatite nanocomposite materials, Mater. Sci. Eng. A 528 (2011) 3689–3696.
[38] R. Ma, L. Weng, X. Bao, Z. Ni, S. Song, W. Cai, Characterization of *in situ* synthesized hydroxyapatite/polyetheretherketone composite materials, Mater. Lett. 71 (2012) 117–119.
[39] R. Ma, L. Weng, L. Fang, Z. Luo, S. Song, Structure and mechanical performance of *in situ* synthesized hydroxyapatite/polyetheretherketone nanocomposite materials, J. Sol-Gel Sci. Technol. 62 (2012) 52–56.
[40] R. Ma, L. Weng, X. Bao, S. Song, Y. Zhang, *In vivo* biocompatibility and bioactivity of *in situ* synthesized hydroxyapatite/polyetheretherketone composite materials, J. Appl. Polym. Sci. 127 (2013) 2581–2587.
[41] T. Tang, R. Ma, S. Tang, H. Tan, W. Lin, Y. Wang, J. Wei, L. Zhao, Preparation, characterization, and *in vitro* osteoblast functions of a nano-hydroxyapatite/polyetheretherketone biocomposite as orthopedic implant material, Int. J. Nanomedicine 9 (2014) 3949–3961.
[42] R. Ma, S. Tang, H. Tan, J. Qian, W. Lin, Y. Wang, C. Liu, J. Wei, T. Tang, Preparation, characterization, *in vitro* bioactivity, and cellular responses to a polyetheretherketone bioactive composite containing nanocalcium silicate for bone repair, ACS Appl. Mater. Interfaces 6 (2014) 12214–12225.
[43] R. Ma, L. Fang, Z. Luo, R. Zheng, S. Song, L. Weng, J. Lei, Fabrication and characterization of modified-hydroxyapatite/polyetheretherketone coating materials, Appl. Surf. Sci. 314 (2014) 341–347.
[44] R. Ma, T. Tang, Current Strategies to Improve the Bioactivity of PEEK, Int. J. Mol. Sci. 15 (2014) 5426–5445.
[45] R. Ma, L. Fang, Z. Luo, L. Weng, S. Song, R. Zheng, H. Sun, H. Fu, Mechanical performance and *in vivo* bioactivity of functionally graded PEEK–HA biocomposite materials, J. Sol-Gel Sci. Technol. 70 (2014) 339–345.
[46] R. Ma, Z. Yu, S. Tang, Y. Pan, J. Wei, T. Tang, Osseointegration of nanohydroxyapatite- or nano-calcium silicate-incorporated polyetheretherketone bioactive composites *in vivo*, Int. J. Nanomedicine 11 (2016) 6023–6033.
[47] R. Ma, Q. Li, L. Wang, X. Zhang, L. Fang, Z. Luo, B. Xue, L. Ma, Mechanical properties and *in vivo* study of modified-hydroxyapatite/polyetheretherketone biocomposites, Mater. Sci. Eng. C 73 (2017) 429–439.
[48] K. Li, C. Y. Yeung, K. W. K. Yeung, S. C. Tjong, Sintered hydroxyapatite/polyetheretherketone nanocomposites: mechanical behavior and biocompatibility, Adv. Eng. Mater. 14 (2012) B155–B165.
[49] K. W. Chan, C. Z. Liao, H. M. Wong, K. W. K. Yeung, S. C. Tjong, Preparation of polyetheretherketone composites with nano-hydroxyapatite rods and carbon nanofibers having high strength, good biocompatibility and excellent thermal stability, RSC Adv. 6 (2016) 19417–19429.

[50] C. Liu, K. Chan, J. Shen, C. Liao, K. Yeung, S. Tjong, Polyetheretherketone hybrid composites with bioactive nanohydroxyapatite and multiwalled carbon nanotube fillers, Polymers 8 (2016) 425.
[51] Y. Pan, Q. Shen, Y. Chen, Fabrication and characterisation of functional gradient hydroxyapatite reinforced poly (ether ether ketone) biocomposites, Micro Nano Lett. 8 (2013) 357–361.
[52] Y. S. Pan, Q. Q. Shen, Y. Chen, K. Yu, C. L. Pan, L. Zhang, Mechanical properties of hydroxyapatite reinforced polyetheretherketone biocomposites, Mater. Technol. Adv. Performance Mater. 30 (2015) 257–263.
[53] Y. Pan, Y. Chen, Q. Shen, Flexural mechanical properties of functional gradient hydroxyapatite reinforced polyetheretherketone biocomposites, J. Mater. Sci. Technol. 32 (2016) 34–40.
[54] L. Wang, S. He, X. Wu, S. Liang, Z. Mu, J. Wei, F. Deng, Y. Deng, S. Wei, Polyetheretherketone/nano-fluorohydroxyapatite composite with antimicrobial activity and osseointegration properties, Biomaterials 35 (2014) 6758–6775.
[55] Y. Deng, X. Liu, A. Xu, L. Wang, Z. Luo, Y. Zheng, F. Deng, J. Wei, Z. Tang, S. Wei, Effect of surface roughness on osteogenesis *in vitro* and osseointegration *in vivo* of carbon fiber-reinforced polyetheretherketone-nanohydroxyapatite composite, Int. J. Nanomedicine 10 (2015) 1425–1447.
[56] A. Xu, X. Liu, X. Gao, F. Deng, Y. Deng, S. Wei, Enhancement of osteogenesis on micro/nano-topographical carbon fiber-reinforced polyetheretherketone–nanohydroxyapatite biocomposite, Mater. Sci. Eng. C 48 (2015) 592–598.
[57] Y. Deng, P. Zhou, X. Liu, L. Wang, X. Xiong, Z. Tang, J. Wei, S. Wei, Preparation, characterization, cellular response and *in vivo* osseointegration of polyetheretherketone/nano-hydroxyapatite/carbon fiber ternary biocomposite, Colloids Surf. B 136 (2015) 64–73.
[58] P. Feng, S. Peng, P. Wu, C. Gao, W. Huang, Y. Deng, T. Xiao, C. Shuai, A nano-sandwich construct built with graphene nanosheets and carbon nanotubes enhances mechanical properties of hydroxyapatite–polyetheretherketone scaffolds, Int. J. Nanomedicine 11 (2016) 3487–3500.
[59] S. Peng, P. Feng, P. Wu, W. Huang, Y. Yang, W. Guo, C. Gao, C. Shuai, Graphene oxide as an interface phase between polyetheretherketone and hydroxyapatite for tissue engineering scaffolds, Sci. Rep. 7 (2017) 46604.
[60] P. Feng, P. Wu, C. Gao, Y. Yang, W. Guo, W. Yang, C. Shuai, A multimaterial scaffold with tunable properties: Toward bone tissue repair, Adv. Sci. (2018) 1700817.
[61] R. K. Roeder, A Paradigm for the integration of biology in materials science and engineering, JOM 62 (2010) 49–55.
[62] M. Garcia-Leiner, M. T. F. Reitman, M. J. El-Hibri, R. K. Roeder, Structure-property relationships in commercial polyetheretherketone resins, Polym. Eng. Sci. 57 (2017) 955–964.
[63] A. R. Boccaccini, C. Peters, J. A. Roether, D. Eifler, S. K. Misra, E. J. Minay, Electrophoretic deposition of polyetheretherketone (PEEK) and PEEK/Bioglass® coatings on NiTi shape memory alloy wires, J. Mater. Sci. 41 (2006) 8152–8159.
[64] I. Y. Kim, A. Sugino, K. Kikuta, C. Ohtsuki, S. B. Cho, Bioactive composites consisting of PEEK and calcium silicate powders, J. Biomater. Appl. 24 (2009) 105–118.
[65] K. L. Wong, C. T. Wong, W. C. Liu, H. B. Pan, M. K. Fong, W. M. Lam, W. L. Cheung, W. M. Tang, K. Y. Chiu, K. D. K. Luk, W. W. Lu, Mechanical properties and *in vitro* response of strontium-containing hydroxyapatite/polyetheretherketone composites, Biomaterials 30 (2009) 3810–3817.
[66] A. R. Rashidi, M. U. Wahit, M. R. Abdullah, Effect of coupling agent on mechanical and biological properties of polyetheretherketone/hydroxyapatite bioactive composite for prosthetic medical device, Key Eng. Mater. 471–472 (2011) 898–903.
[67] B. J. Meenan, C. McClorey, M. Akay, Thermal analysis studies of poly(etheretherketone)/hydroxyapatite biocomposite mixtures, J. Mater. Sci. Mater. Med. 11 (2000) 481–489.
[68] C.-T. Han, M. Chi, Y.-Y. Zheng, L.-X. Jiang, C.-D. Xiong, L.-F. Zhang, Mechanical properties and bioactivity of high-performance poly(etheretherketone)/carbon nanotubes/bioactive glass biomaterials, J. Polym. Res. 20 (2013) 203.

[69] J. Cao, Y. Lu, H. Chen, L. Zhang, C. Xiong, Preparation, properties and *in vitro* cellular response of multi-walled carbon nanotubes/bioactive glass/poly(etheretherketone) biocomposite for bone tissue engineering, Int. J. Polym. Mater. Polym. Biomater. (2018)

[70] H.-D. Jung, H.-S. Park, M.-H. Kang, Y. Li, H.-E. Kim, Y.-H. Koh, Y. Estrin, Reinforcement of polyetheretherketone polymer with titanium for improved mechanical properties and *in vitro* biocompatibility, J. Biomed. Mater. Res. 104B (2016) 141–148.

[71] M. Vaezi, S. Yang, A novel bioactive PEEK/HA composite with controlled 3D interconnected HA network, Int. J. Bioprinting 1 (2015) 66–76.

[72] M. Vaezi, C. Black, D. Gibbs, R. Oreffo, M. Brady, M. Moshrefi-Torbati, S. Yang, Characterization of new PEEK/HA composites with 3D HA network fabricated by extrusion freeforming, Molecules 21 (2016) 687.

[73] P. Roy, R. R. N. Sailaja, Mechanical, thermal and bio-compatibility studies of PAEK-hydroxyapatite nanocomposites, J. Mech. Behav. Biomed. Mater. 49 (2015) 1–11.

[74] B. T. Rego, W. A. R. Neto, A. C. C. de Paula, A. M. Góes, R. E. S. Bretas, Mechanical properties and stem cell adhesion of injection-molded poly(ether ether ketone) and hydroxyapatite nanocomposites, J. Appl. Polym. Sci. 132 (2015) 41748.

[75] B. Yuan, Y. Chen, H. Lin, Y. Song, X. Yang, H. Tang, E. Xie, T. Hsu, X. Yang, X. Zhu, K. Zhang, X. Zhang, Processing and properties of bioactive surface-porous PEKK, ACS Biomater. Sci. Eng. 2 (2016) 977–986.

[76] B. Yuan, Q. Cheng, R. Zhao, X. Zhu, X. Yang, X. Yang, K. Zhang, Y. Song, X. Zhang, Comparison of osteointegration property between PEKK and PEEK: Effects of surface structure and chemistry, Biomaterials 170 (2018) 116–126.

[77] D. Rajeswari, D. Gopi, S. Ramya, L. Kavitha, Investigation of anticorrosive, antibacterial and *in vitro* biological properties of a sulphonated poly(etheretherketone)/strontium, cerium co-substituted hydroxyapatite composite coating developed on surface treated surgical grade stainless steel for orthopedic applications, RSC Adv. 4 (2014) 61525–61536.

[78] H. McDowell, T. M. Gregory, W. E. Brown, Solubility of $Ca_5(PO_4)_3OH$ in the System $Ca(OH)_2$–$H_3PO_4$–$H_2O$ at 5, 15, 25, and 37°C, J. Res. Natl. Bur. Stand. 81A (1977) 273–281.

[79] F. C. M. Driessens, R. M. H. Verbeeck, Biominerals, CRC Press, Boca Raton, FL, 1990.

[80] A. Kalambettu, S. Dharmalingam, Fabrication and *in vitro* evaluation of sulphonated polyether ether ketone/nano hydroxyapatite composites as bone graft materials, Mater. Chem. Phys. 147 (2014) 168–177.

[81] J. C. Moreno, M. Kresak, R. T. Zahradnik, Physiochemical aspects of fluoride-apatite systems relevant to the study of dental caries, Caries Res. 11 (1977) 142–171.

[82] T. M. Gregory, E. C. Moreno, J. M. Patel, W. E. Brown, Solubility of β-$Ca_3(PO_4)_2$ in the system $Ca(OH)_2$–$H_3PO_4$–$H_2O$ at 5, 15, 25 and 37°C, J. Res. Natl. Bur. Stand. 78A (1974) 667–674.

[83] F. P. Glasser, E. E. Lachowski, D. E. Macphee, Compositional model for calcium silicate hydrate (C-S-H) gels, their solubilities, and free energies of formation, J. Am. Ceram. Soc. 70 (1997) 481–485.

[84] L. Cai, Y. Pan, S. Tang, Q. Li, T. Tang, K. Zheng, A. R. Boccaccini, S. Wei, J. Wei, J. Su, Macro-mesoporous composites containing PEEK and mesoporous diopside as bone implants: characterization, *in vitro* mineralization, cytocompatibility, and vascularization potential and osteogenesis *in vivo*, J. Mater. Chem. B 8 (2017) 8337–8352.

[85] J. Zhang, W. Wei, L. Yang, Y. Pan, X. Wang, T. Wang, S. Tang, Y. Yao, H. Hong, J. Wei, Stimulation of cell responses and bone ingrowth into macro-microporous implants of nano-bioglass/polyetheretherketone composite and enhanced antibacterial activity by release of hinokitiol, Colloids Surf. B 164 (2018) 347–357.

[86] R. K. Roeder, T. L. Conrad, Bioactive polyaryletherketone composites, in: S. M. Kurtz (Ed.), PEEK Biomaterials Handbook, Elsevier Inc., Amsterdam, 2012, , pp. 163–179.

[87] T. Okuda, K. Ioku, I. Yonezawa, H. Minagi, Y. Gonda, G. Kawachi, M. Kamitakahara, Y. Shibata, H. Murayama, H. Kurosawa, T. Ikeda, The slow resorption with replacement of bone by a hydrothermally synthesized pure calcium-deficient hydroxyapatite, Biomaterials 29 (2008) 2719–2728.

[88] W. Suchanek, M. Yoshimura, Processing and properties of hydroxyapatite-based biomaterials for use as hard tissue replacement implants, J. Mater. Res. 13 (1998) 94–109.

[89] R. K. Roeder, G. L. Converse, H. Leng, W. Yue, Kinetic effects on hydroxyapatite whiskers synthesized by the chelate decomposition method, J. Am. Ceram. Soc. 89 (2006) 2096–2104.
[90] I. S. Neira, Y. V. Kolen'ko, O. I. Lebedev, G. Van Tendeloo, H. S. Gupta, F. Guitián, M. Yoshimura, An effective morphology control of hydroxyapatite crystals via hydrothermal synthesis, Cryst. Growth Des. 9 (2009) 466–474.
[91] A. C. Tas, Molten Salt synthesis of calcium hydroxyapatite whiskers, J. Am. Ceram. Soc. 84 (2001) 295–300.
[92] L. Yubao, K. de Groot, J. de Wijn, C. P. A. T. Klein, S. V. D. Meer, Morphology and composition of nanograde calcium phosphate needle-like crystals formed by simple hydrothermal treatment, J. Mater. Sci. Mater. Med. 5 (1994) 326–331.
[93] K. Teraoka, A. Ito, K. Onuma, T. Tateishi, S. Tsutsumi, Hydrothermal growth of hydroxyapatite single crystals under natural convection, J. Mater. Res. 14 (1999) 2655–2661.
[94] S.-L. Gao, J.-K. Kim, Cooling rate influences in carbon fibre/PEEK composites. Part 1. Crystallinity and interface adhesion, Composites 31A (2000) 517–530.
[95] S. Kasahara, T. Sawamura, Article with foamed surface, implant and method of producing the same, U.S. Patent No. 9,931, 438, 2018.
[96] A. H. C. Poulsson, D. Eglin, S. Zeiter, K. Camenisch, C. Sprecher, Y. Agarwal, D. Nehbass, J. Wilson, R. G. Richards, Osseointegration of machined, injection moulded and oxygen plasma modified PEEK implants in a sheep model, Biomaterials 35 (2014) 3717–3728.
[97] S. W. Ha, M. Kirch, F. Birchler, K. L. Ekert, J. Mayer, E. Wintermantel, C. Sittig, I. Pfund-Klingenfuss, M. Textor, N. D. Spencer, M. Guecheva, H. Bonmont, Surface activation of polyetheretherketone (PEEK) and formation of calcium phosphate coatings by precipitation, J. Mater. Sci. Mater. Med. 8 (1997) 683–690.
[98] ASTM C373-88, Standard test method for water absorption, bulk density, apparent porosity, and apparent specific gravity of fired whiteware products, American Society for Testing and Materials, West, Conshohocken, PA, 2006.
[99] ASTM D792-13, Standard test methods for density and specific gravity (relative density) of plastics by displacement, American Society for Testing and Materials, West, Conshohocken, PA, 2013.
[100] ASTM D3418-08, Standard Test Method for Transition Temperatures and Enthalpies of Fusion and Crystallization of Polymers by Differential Scanning Calorimetry, American Society for Testing and Materials, West, Conshohocken, PA, 2008.
[101] ASTM F2778-09, Standard test method for measurement of percent crystallinity of polyetheretherketone (PEEK) polymers by means of specular reflectance Fourier transform infrared spectroscopy (R-FTIR), American Society for Testing and Materials, West Conshohocken, PA, 2009.
[102] J. C. Russ, R. T. Dehoff, Practical Stereology, Springer, New York, NY, 2000.
[103] W. Yue, R. K. Roeder, Micromechanical model for hydroxyapatite whisker reinforced polymer biocomposites, J. Mater. Res. 21 (2006) 2136–2145.
[104] ASTM F2450-10, Standard guide for assessing microstructure of polymeric scaffolds for use in tissue-engineered medical products, American Society for Testing and Materials, West Conshohocken, PA, 2010.
[105] L. M. Wenz, K. Merrit, S. A. Brown, A. Moet, A. D. Steffee, *In vitro* biocompatibility of polyetheretherketone and polysulfone composites, J. Biomed. Mater. Res. 24 (1990) 207–215.
[106] K. A. Jockisch, S. A. Brown, T. W. Bauer, K. Merritt, Biological response to chopped-carbon-fiber-reinforced peek, J. Biomed. Mater. Res. 26 (1992) 133–146.
[107] C.-H. Rivard, S. Rhalmi, C. Coillard, *In vivo* biocompatibility testing of peek polymer for a spinal implant system: a study in rabbits, J. Biomed. Mater. Res. 62 (2002) 488–498.
[108] T. Nieminen, I. Kallela, E. Wuolijoki, H. Kainulainen, I. Hiidenheimo, I. Rantala, Amorphous and crystalline polyetheretherketone: mechanical properties and tissue reactions during a 3-year follow-up, J. Biomed. Mater. Res. 84A (2008) 377–383.
[109] K. B. Sagomonyants, M. L. Jarman-Smith, J. N. Devine, M. S. Aronow, G. A. Gronowicz, The *in vitro* response of human osteoblasts to

polyetheretherketone (PEEK) substrates compared to commercially pure titanium, Biomaterials 29 (2008) 1563–1572.
[110] J. W. Brantigan, P. C. McAfee, B. W. Cunningham, H. Wang, C. M. Orbegoso, Interbody lumbar fusion using a carbon fiber cage implant versus allograft bone, Spine 19 (1994) 1436–1444.
[111] H. Oguchi, K. Ishikawa, K. Mizoue, K. Seto, G. Eguchi, Long-term histological evaluation of hydroxyapatite ceramics in humans, Biomaterials 16 (1995) 33–38.
[112] R. Z. LeGeros, Properties of osteoconductive biomaterials: Calcium phosphates, Clin. Orthop. Relat. Res. (2002) 81–98.
[113] P. Habibovic, K. de Groot, Osteoinductive biomaterials—properties and relevance in bone repair, J. Tissue Eng. Regen. Med. 1 (2007) 25–32.
[114] U. Ripamonti, Osteoinduction in porous hydroxyapatite implanted in heterotopic sites of different animal models, Biomaterials 17 (1996) 31–35.
[115] A. K. Gosain, L. Song, P. Riordan, M. T. Amarante, P. G. Nagy, C. R. Wilson, J. M. Toth, J. L. Ricci, A 1-year study of osteoinduction in hydroxyapatite-derived biomaterials in an adult sheep model: part I, Plast. Reconstr. Surg. 106 (2002) 619–630.
[116] M. J. Meagher, H. E. Weiss-Bilka, M. E. Best, D. R. Wagner, R. K. Roeder, Acellular hydroxyapatite-collagen scaffolds support angiogenesis and osteogenic gene expression in an ectopic murine model: effects of hydroxyapatite volume fraction, J. Biomed. Mater. Res. 104A (2016) 2178–2188.
[117] R. Shu, R. McMullen, M. J. Baumann, L. R. McCabe, Hydroxyapatite accelerates differentiation and suppresses growth of MC3T3-E1 osteoblasts, J. Biomed. Mater. Res. 67A (2003) 1196–1204.
[118] J. Wiltfang, H. A. Merten, K. A. Schlegel, S. Schultze-Mosgau, F. R. Kloss, S. Rupprecht, P. Kessler, Degradation characteristics of α and β tri-calcium-phosphate (TCP) in minipigs, J. Biomed. Mater. Res. 63B (2002) 115–121.
[119] N. Patel, S. M. Best, W. Bonfield, I. R. Gibson, K. A. Hing, E. Damien, P. A. Revell, A comparative study on the *in vivo* behavior of hydroxyapatite and silicon substituted hydroxyapatite granules, J. Mater. Sci. Mater. Med. 13 (2002) 1199–1206.
[120] H.-J. Cha, C. W. Frank, Annealing study of poly(ether ether ketone): Temperature effect on molecular conformation and crystallinity, Korea Polym. J. 7 (1999) 141–149.
[121] J. P. Fan, C. P. Tsui, C. Y. Tang, C. L. Chow, Influence of interphase layer on the overall elasto-plastic behaviors of HA/PEEK biocomposite, Biomaterials 25 (2004) 5363–5373.
[122] J. P. Fan, C. P. Tsui, C. Y. Tang, Modeling of the mechanical behavior of HA/PEEK biocomposite under quasi-static tensile load, Mater. Sci. Eng. A 382 (2004) 341–350.
[123] C. Y. Tang, C. P. Tsui, W. Lin, P. S. Uskokovic, Z. W. Wang, Multi-level finite element analysis for progressive damage behavior of HA/PEEK composite porous structure, Compos. Part B 55 (2013) 22–30.
[124] R. K. Roeder, M. S. Sproul, C. H. Turner, Hydroxyapatite whiskers provide improved mechanical properties in reinforced polymer composites, J. Biomed. Mater. Res. 67A (2003) 801–812.
[125] L. Fang, Y. Leng, P. Gao, Processing and mechanical properties of HA/UHMWPE nanocomposites, Biomaterials 27 (2006) 3701–3707.
[126] M. E. Islas-Blancas, J. M. Cervantes-Uc, R. Vargas-Coronado, J. V. Cauich-Rodríguez, R. Vera-Graziano, A. Martinez-Richa, Characterization of bone cements prepared with functionalized methacrylates and hydroxyapatite, J. Biomater. Sci. Polymer Ed. 12 (2001) 893–910.
[127] A. Canul-Chuil, R. Vargas-Coronado, J. V. Cauich-Rodríguez, A. Martinez-Richa, E. Fernández, S. N. Nazhat, Comparative study of bone cements prepared with either HA or α-TCP and functionalized methacrylates, J. Biomed. Mater. Res. 64B (2003) 27–37.
[128] L. Morejón, A. E. Mendizábal, J. A. D. García-Menocal, M. P. Ginebra, C. Aparicio, F. J. G. Mur, M. Marshal, N. Davidenko, M. E. Ballesteros, J. A. Planell, Static mechanical properties of hydroxyapatite (HA) powder-filled acrylic bone cements: Effect of type of HA powder, J. Biomed. Mater. Res. 72B (2005) 345–352.

[129] M. Saito, A. Maruoka, T. Mori, N. Sugano, K. Hino, Experimental studies on a new bioactive bone cement: hydroxyapatite composite resin, Biomaterials 15 (1994) 156–160.
[130] R. Labella, M. Braden, S. Deb, Novel hydroxyapatite-based dental composites, Biomaterials 15 (1994) 1197–1200.
[131] M. Kobayashi, T. Nakamura, S. Shinzato, W. F. Mousa, K. Nishio, K. Ohsawa, T. Kokubo, T. Kikutani, Effect of bioactive filler content on mechanical properties and osteoconductivity of bioactive bone cement, J. Biomed. Mater. Res. 46 (1999) 447–457.
[132] C. Santos, Z. B. Luklinska, R. L. Clarke, K. W. M. Davy, Hydroxyapatite as a filler for dental composite materials: mechanical properties and *in vitro* bioactivity of composites, J. Mater. Sci. Mater. Med. 12 (2001) 565–573.
[133] Y. Shikinami, M. Okuno, Bioresorbable devices made of forged composites of hydroxyapatite (HA) particles and poly-L-lactide (PLLA): Part I. Basic characteristics, Biomaterials 20 (1999) 859–877.
[134] Z. Hong, P. Zhang, C. He, X. Qiu, A. Liu, L. Chen, X. Chen, X. Jing, Nano-composite of poly(L-lactide) and surface grafted hydroxyapatite: mechanical properties and biocompatibility, Biomaterials 26 (2005) 6296–6304.
[135] N. H. Ladizesky, E. M. Pirhonen, D. B. Appleyard, I. M. Ward, W. Bonfield, Fibre reinforcement of ceramic/polymer composites for a major load-bearing bone substitute material, Compos. Sci. Technol. 58 (1998) 419–434.
[136] W. J. McGregor, K. E. Tanner, W. Bonfield, M. Bonner, L. S. Saunders, I. M. Ward, Fatigue properties of isotropic and hydrostatically extruded HAPEX$^{TM}$, J. Mater. Sci. Lett. 19 (2000) 1787–1788.
[137] M. Bonner, L. S. Saunders, I. M. Ward, G. W. Davies, M. Wang, K. E. Tanner, W. Bonfield, Anisotropic mechanical properties of oriented HAPEX$^{TM}$, J. Mater. Sci. 37 (2002) 325–334.
[138] R. A. Sousa, R. L. Reis, A. M. Cunha, M. J. Bevis, Processing and properties of ? bone-analogue? biodegradable and bioinert polymer composites, Compos. Sci. Technol. 63 (2003) 389–402.
[139] D. T. Reilly, A. H. Burstein, The elastic and ultimate properties of compact bone tissue, J. Biomech. 8 (1975) 393–405.
[140] S. C. Cowin (Ed.), Bone Mechanics Handbook, CRC Press, Boca Raton, FL, 2001.
[141] E. F. Morgan, T. M. Keaveny, Dependence of yield strain of human trabecular bone on anatomic site, J. Biomech. 34 (2001) 569–577.
[142] T. M. Keaveny, E. F. Morgan, G. L. Niebur, O. C. Yeh, Biomechanics of trabecular bone, Annu. Rev. Biomed. Eng. 3 (2001) 307–333.
[143] R. J. Kane, G. L. Converse, R. K. Roeder, Effects of the reinforcement morphology on the fatigue properties of hydroxyapatite reinforced polymers, J. Mech. Behav. Biomed. Mater. 1 (2008) 261–268.
[144] FDA Public Health Notification: Life-threatening complications associated with recombinant human bone morphogenetic protein in cervical spine fusion, July 1, 2008.
[145] K. Burkus Jr., Early outcomes of anterior cervical discectomy and fusion using a porous PEEK interbody fusion device, J. Spine Neurosurg. 7 (2018) 1000295.